

ผลของสเตอโรลเพปไทด์เกลียวแอลฟามาสเตอร์โมดูล์ 1 (SAHM1) คอนจูเกตกับอนุภาคทองระดับนาโนต่อวิถีสัญญาณ NOTCH ในเซลล์มะเร็งเม็ดเลือดขาว JURKAT ของมนุษย์



นางสาวชลนิชา สืบโกฏ

จุฬาลงกรณ์มหาวิทยาลัย

บทคัดย่อและแฟ้มข้อมูลฉบับเต็มของวิทยานิพนธ์ตั้งแต่ปีการศึกษา 2554 ที่ให้บริการในคลังปัญญาจุฬาฯ (CUIR) เป็นแฟ้มข้อมูลของนิสิตเจ้าของวิทยานิพนธ์ ที่ส่งผ่านทางบัณฑิตวิทยาลัย

The abstract and full text of theses from the academic year 2011 in Chulalongkorn University Intellectual Repository (CUIR) are the thesis authors' files submitted through the University Graduate School.

วิทยานิพนธ์นี้เป็นส่วนหนึ่งของการศึกษาตามหลักสูตรปริญญาวิทยาศาสตรมหาบัณฑิต

สาขาวิชาเทคโนโลยีชีวภาพ

คณะวิทยาศาสตร์ จุฬาลงกรณ์มหาวิทยาลัย

ปีการศึกษา 2560

ลิขสิทธิ์ของจุฬาลงกรณ์มหาวิทยาลัย

EFFECT OF STAPLED α -HELICAL MASTERMIND LIKE 1 (SAHM1)
PEPTIDE CONJUGATED WITH GOLD NANOPARTICLES TOWARD NOTCH SIGNALING
PATHWAY IN HUMAN LEUKEMIA JURKAT CELL



A Thesis Submitted in Partial Fulfillment of the Requirements
for the Degree of Master of Science Program in Biotechnology

Faculty of Science

Chulalongkorn University

Academic Year 2017

Copyright of Chulalongkorn University

Thesis Title EFFECT OF STAPLED α -HELICAL MASTERMIND
LIKE 1 (SAHM1) PEPTIDE CONJUGATED WITH GOLD
NANOPARTICLES TOWARD NOTCH SIGNALING
PATHWAY IN HUMAN LEUKEMIA JURKAT CELL

By Miss Chonnicha Subkod

Field of Study Biotechnology

Thesis Advisor Associate Professor Tanapat Palaga, Ph.D.

Thesis Co-Advisor Associate Professor Kittinan Komolpis, Ph.D.
Assistant Professor Stephan T.dubas, Ph.D.

Accepted by the Faculty of Science, Chulalongkorn University in Partial
Fulfillment of the Requirements for the Master's Degree

.....Dean of the Faculty of Science
(Professor Polkit Sangvanich, Ph.D.)

THESIS COMMITTEE

.....Chairman
(Assistant Professor Kobchai Pattaragulwanit, Dr.rer.nat.)

.....Thesis Advisor
(Associate Professor Tanapat Palaga, Ph.D.)

.....Thesis Co-Advisor
(Associate Professor Kittinan Komolpis, Ph.D.)

.....Thesis Co-Advisor
(Assistant Professor Stephan T.dubas, Ph.D.)

.....Examiner
(Associate Professor Chanpen Chanchao, Ph.D.)

.....External Examiner
(Associate Professor Primchanien Moongkarndi, Ph.D.)

ชลนิชา สืบโกฏ : ผลของสเตพิลด์เพปไทด์เกลียวแอลฟามาสเตอร์ไมด์ไลค์ 1 (SAHM1) คอนจูเกตกับอนุภาคทองคำระดับนาโนต่อวิถีสัญญาณ NOTCH ในเซลล์มะเร็งเม็ดเลือดขาว JURKAT ของมนุษย์ (EFFECT OF STAPLED α -HELICAL MASTERMIND LIKE 1 (SAHM1) PEPTIDE CONJUGATED WITH GOLD NANOPARTICLES TOWARD NOTCH SIGNALING PATHWAY IN HUMAN LEUKEMIA JURKAT CELL) อ.ที่ปรึกษาวิทยานิพนธ์หลัก: รศ. ดร. ธนาภัทร ปาลกะ, อ.ที่ปรึกษาวิทยานิพนธ์ร่วม: รศ. ดร. กิตตินันท์ โกมลภิส, ผศ. ดร. สเดฟาน ที ดูบาส, 73 หน้า.

ในปัจจุบัน โรคมะเร็งเป็นสาเหตุการตายสูงสุดของประเทศไทย ซึ่งโรคมะเร็งเกิดจากความผิดปกติในการแบ่งตัวของเซลล์อย่างไร้การควบคุม สำหรับโรคมะเร็งเม็ดเลือดขาว (leukemia) ชนิด T-cell acute lymphoblastic leukemia (T-ALL) พบว่ายีนที่ประมวลรหัสโปรตีน Notch มักมีการกลายพันธุ์ ทำให้วิถีสัญญาณ Notch มีการทำงานตลอดเวลา การทำงานของวิถี Notch ตลอดเวลานี้เป็นปัจจัยขับเคลื่อนให้เซลล์เกิดการแบ่งตัวแบบไม่หยุดยั้ง การรักษาโรคมะเร็งมีด้วยกันหลายวิธี เช่น การผ่าตัด เคมีบำบัด เป็นต้น แต่การรักษาเหล่านี้ยังคงมีผลข้างเคียง ดังนั้น จึงได้มีการพัฒนาระบบการนำส่งยาแบบจำเพาะต่อเซลล์เป้าหมาย ในการศึกษาครั้งนี้มีวัตถุประสงค์เพื่อพัฒนาระบบนำส่งยาโดยใช้อนุภาคทองคำระดับนาโน (AuNP) เป็นตัวนำส่งสเตพิลด์เพปไทด์เกลียวแอลฟามาสเตอร์ไมด์ไลค์ 1 (SAHM1) ไปยับยั้งการทำงานของวิถีสัญญาณ Notch ในเซลล์มะเร็งเม็ดเลือดขาว โดยใช้เซลล์ไลน์ Jurkat เป็นต้นแบบในการศึกษา SAHM1 มีขนาดโมเลกุลที่เล็กกว่าโปรตีนทั่วไปและสามารถถูกดูดซึมเข้าสู่เซลล์ได้อย่างรวดเร็ว ในการทดสอบความเป็นพิษโดยวิธี MTT พบว่า ค่าความเข้มข้นที่ให้ผลเปอร์เซ็นต์การมีชีวิตรอดของเซลล์ครึ่งหนึ่ง (IC_{50}) ของ SAHM1 ต่อ Jurkat เท่ากับ 17.54 ± 5.17 ไมโครโมลาร์ ณ เวลา 72 ชั่วโมง การคอนจูเกต SAHM1 กับ AuNP ใช้ thiol PEG เป็นตัวเชื่อมให้ติดกัน (SAHM1-PEG-AuNP) ที่ความเข้มข้น 16.25, 31.3 และ 62.5 ไมโครโมลาร์ และนำไปวัด UV-Visible spectroscopy พบว่าความยาวคลื่นสูงสุดที่เปลี่ยนไปของ SAHM1-PEG-AuNP เท่ากับ 527 นาโนเมตรเมื่อเทียบกับความยาวคลื่นสูงสุดของ AuNP เท่ากับ 523 นาโนเมตร แสดงว่า SAHM1 คอนจูเกตติดกับ AuNP สำเร็จแล้ว เมื่อนำมาทดสอบความเป็นพิษโดยวิธี MTT พบว่า ความเป็นพิษของ SAHM1-PEG-AuNP เพิ่มขึ้นอย่างมีนัยสำคัญ เมื่อเปรียบเทียบกับ SAHM1 ที่ไม่ได้คอนจูเกต สำหรับการศึกษาตำแหน่งภายในเซลล์ของ SAHM1-PEG-AuNP โดยใช้กล้องจุลทรรศน์อิเล็กตรอนแบบส่องผ่าน (TEM) พบว่า SAHM1-PEG-AuNP อยู่ในไซโทพลาสซึมของเซลล์ ในขณะที่ AuNP เพียงอย่างเดียวไม่สามารถเข้าสู่เซลล์ได้ ในการศึกษาผลของ SAHM1-PEG-AuNP ต่อวิถีสัญญาณ Notch ด้วยวิธี qPCR ในยีนเป้าหมายของ Notch (*HES1*, *HEY1* and *MYC*) พบว่าระดับการแสดงออกของ SAHM1-PEG-AuNP ลดต่ำลงในเซลล์ที่ได้รับ จากการทดลองทั้งหมดแสดงให้เห็นว่า AuNP เป็นตัวพา SAHM1 ไปยับยั้งการทำงานของยีน Notch ทำให้สามารถยับยั้งการเจริญของเซลล์มะเร็งได้ ซึ่งใช้เป็นแนวทางนำไปสู่การผลิตยาและการรักษามะเร็งแนวใหม่ในอนาคตต่อไป

สาขาวิชา เทคโนโลยีชีวภาพ

ปีการศึกษา 2560

ลายมือชื่อนิสิต

ลายมือชื่อ อ.ที่ปรึกษาหลัก

ลายมือชื่อ อ.ที่ปรึกษาร่วม

ลายมือชื่อ อ.ที่ปรึกษาร่วม

5871933323 : MAJOR BIOTECHNOLOGY

KEYWORDS: GOLD NANOPARTICLE / SAHM1 PEPTIDE / NOTCH SIGNALING PATHWAY

CHONNICHIA SUBKOD: EFFECT OF STAPLED α -HELICAL MASTERMIND LIKE 1 (SAHM1) PEPTIDE CONJUGATED WITH GOLD NANOPARTICLES TOWARD NOTCH SIGNALING PATHWAY IN HUMAN LEUKEMIA JURKAT CELL. ADVISOR: ASSOC. PROF. TANAPAT PALAGA, Ph.D., CO-ADVISOR: ASSOC. PROF. KITTINAN KOMOLPIS, Ph.D., ASST. PROF. STEPHAN T.DUBAS, Ph.D., 73 pp.

Currently, cancer is the top cause of death in Thailand and caused by the growth and spreading of abnormal cells in an uncontrolled manner. For T-cell acute lymphoblastic leukemia (T-ALL), it was found that gene of encoding protein Notch is often mutated. In T-ALL, Notch signaling pathway is hyperactivated resulting in uncontrolled cell division. There are many types of cancer treatment such as surgery and chemotherapy but both approaches have serious side effects. Therefore, development of target drug delivery system is needed. In this study, the objective was to develop specific target drug delivery system by using gold nanoparticle (AuNP) as a vector of stapled α -helical peptide from Mastermind-like1 (SAHM1) for inhibition of Notch signaling pathway in T cell leukemia cell line (Jurkat), SAHM1 is smaller than its original protein and rapidly absorbed into cells. In cytotoxicity test by MTT assay, the 50% inhibition concentration (IC_{50}) of SAHM1 against Jurkat cell was $17.54 \pm 5.17 \mu\text{M}$ at 72 h. Conjugation of SAHM1 to AuNP linked by polyethylene glycol (SAHM1-PEG-AuNP) at the concentration of 16.25, 31.3 and 62.5 μM was characterized by UV-Visible spectroscopy. The result showed the shift peak of the conjugate at 527 nm, when compared with the 523 nm peak of 40 nm AuNP. This result indicated that SAHM1 was successfully conjugated to AuNP. In the cytotoxicity test by MTT assay, the cytotoxicity of SAHM1-PEG-AuNP was increased significantly when compared with unconjugated SAHM1. Cellular uptake and localization was detected by transmission electron microscope (TEM). The result demonstrated that SAHM1-PEG-AuNP localized in the cytoplasm of Jurkat cell line, while unconjugated AuNP was found outside of Jurkat cell line. The effect of SAHM1-PEG-AuNP on Notch signaling pathway was measured by qPCR of the Notch target genes (*HES1*, *HEY1* and *MYC*). The result showed that the mRNA level of Notch target genes in SAHM1-PEG-AuNP treated cells did not significantly decrease. Collectively, these results indicated that AuNP could be used as the cell-penetrating carrier of SAHM1 in order to kill cancer cell lines. This result opens a new way for drug and new cancer treatment in the future.

Field of Study: Biotechnology

Academic Year: 2017

Student's Signature

Advisor's Signature

Co-Advisor's Signature

Co-Advisor's Signature

ACKNOWLEDGEMENTS

This thesis could not be successfully completed without the support of many people. First and foremost, I would like to thank my thesis advisor, Assoc. Prof. Dr. Tanapat Palaga, who supervised this thesis. Furthermore, I would like to thank my co-advisor Assoc. Prof. Dr. Kittinan Komolpis and Asst. Prof. Dr. Stephan Thierry Dubas for their invaluable help, suggestion and encouragement throughout this research.

In addition, I also express my deepest gratitude to all thesis committee, Asst. Prof. Dr. Kobchai Pattaragulwanit, Assoc. Prof. Dr. Chanpen Chanchao, and Assoc. Prof. Dr. Primchanien Moongkarndi, external committee from Department of Microbiology, Faculty of Pharmacy, Mahidol University, for their comments and suggestions which greatly assisted to improve completely my thesis.

I would like to express my deep appreciation to Mrs. Songchan Puthong and Mr. Anumart Buakeaw for their abundantly helpful, invaluable assistance, support and guidance.

Finally, I would like to thank my parents, friends and all members at Institute of Biotechnology and Genetic Engineering, Chulalongkorn University for their full support friendship and helpfulness.

CONTENTS

	Page
THAI ABSTRACT	iv
ENGLISH ABSTRACT	v
ACKNOWLEDGEMENTS	vi
CONTENTS.....	vii
LIST OF TABLES	xi
LIST OF FIGURES.....	xii
LIST OF ABBREVIATIONS	xvi
CHAPTER I	1
INTRODUCTION	1
1.1 Rationale.....	1
1.2 Objective of the Study.....	2
1.3 Scope of the Study.....	2
1.4 Advantage of the Study.....	2
CHAPTER II.....	3
LITERATURE REVIEWS.....	3
2.1 Cancer	3
2.1.1 Causes of cancer.....	3
2.1.2 Types of cancer.....	4
2.1.3 Cancer treatment.....	5
2.2 Leukemia	7
2.3 Stapled α -helical peptide of Mastermind-like 1 (SAHM1).....	9

	Page
2.3.1 Notch signaling pathway	9
2.3.2 Design and synthesis of SAHM1	11
2.3.3 Functions of SAHM1	14
2.3.4 Stapled peptide in cancer therapy	15
2.4 Gold nanoparticle	16
2.4.1 History of nanoparticle	16
2.4.2 Applications of gold nanoparticle in biological and medical	17
2.4.3 Synthesis of gold nanoparticle	18
2.4.4 Method of conjugation protein and peptide to gold nanoparticle	20
2.5 Jurkat cell line	22
CHAPTER III	23
MATERIALS AND METHODS	23
3.1 Chemicals and reagents	23
3.2 Equipments	24
3.3 Experimental procedures	26
Part I Preparation of SAHM1-PEG -gold nanoparticle conjugate	26
3.3.1 Optimization of SAHM1 peptide for conjugate on gold nanoparticle	26
3.3.2 Conjugation of SAHM1-PEG-gold nanoparticle	26
Part II Cytotoxicity of SAHM1-PEG-AuNP	28
3.3.3 Cell culture	28
3.3.4 Cytotoxicity assay	28
Part III Internalization and localization of SAHM1-PEG-AuNP in cells	30

	Page
Part IV Effect of SAHM1-AuNP on Notch signaling pathway.....	30
3.3.7 Cell culture.....	30
3.3.8 RNA extraction and quantitative RT-PCR.....	30
3.3.9 Statistical analysis.....	32
CHAPTER IV.....	33
RESULTS AND DISCUSSION.....	33
Part I Preparation of SAHM1-PEG-gold nanoparticle conjugate (SAHM1-PEG-AuNP).....	33
4.1 Optimization of SAHM1 peptide for conjugation on gold nanoparticle.....	33
4.2 Preparation and characterization of SAHM1-PEG-gold nanoparticle conjugate (SAHM1-PEG-AuNP).....	34
Part II Cytotoxicity test.....	37
4.3 Cytotoxicity of the unconjugate SAHM1.....	37
4.4 Cytotoxicity of DAPT.....	40
4.5 Cytotoxicity of gold nanoparticle.....	42
4.6 Cytotoxicity of PEG.....	44
4.7 Cytotoxicity of SAHM1-PEG-AuNP.....	46
Part III Internalization and localization of SAHM1-PEG-AuNP.....	50
Part IV Effect of SAHM1-PEG-AuNP on Notch signaling pathway.....	55
CHAPTER V.....	57
CONCLUSION.....	57
REFERENCES.....	58
APPENDICES.....	62
APPENDIX A.....	63

	Page
APPENDIX B.....	65
APPENDIX C.....	67
APPENDIX D.....	71
VITA	73



LIST OF TABLES

Table 2.1 Sequences and helical character of MAML1-derived SAHM peptides.... 12

Table 2.2 Examples of biomedical applications of gold nanoparticle..... 18

Table 3.1 Realtime PCR primer name and sequence.....32



LIST OF FIGURES

Figure 2.1 Development of normal cells to cancer cells.	3
Figure 2.2 Risk factors of cancer.....	4
Figure 2.3 Cancer types of human worldwide.....	5
Figure 2.4 Cancer treatment from past to present.....	6
Figure 2.5 Morphology of abnormally white blood cell in leukemia.....	8
Figure 2.6 Experimental manipulation of Notch signaling pathway.....	10
Figure 2.7 Process of SAHM1 inhibiting the Notch signaling pathway.....	11
Figure 2.8 Structure of SAHM1 peptide.....	12
Figure 2.9 Design of stapled peptides targeting the Notch/CSL complex.	13
Figure 2.10 Molecular structure of SAHM1 peptide.	14
Figure 2.11 Functions of stapled peptide.....	14
Figure 2.12 Formation of gold nanoparticle by the sodium borohydride capping..	19
Figure 2.13 Synthesis of gold nanoparticle by Turkevich method.....	20
Figure 2.14 Hydrophobic and ionic interactions between peptide (blue) and gold nanoparticle surface (orange).	21
Figure 2.15 Morphology of Jurkat cell line.....	22
Figure 3.1 Predicted formation of SAHM1-gold nanoparticle conjugate.....	27
Figure 3.2 Shift in surface plasmon absorption of AuNP (40 nm) due to protein conjugation.....	27
Figure 3.3 Chemical structure of the yellow dye (MTT) and the converted to a purple formazan in living cells.....	28
Figure 3.4 Example of inhibitory concentration (IC_{50}) curve.....	29

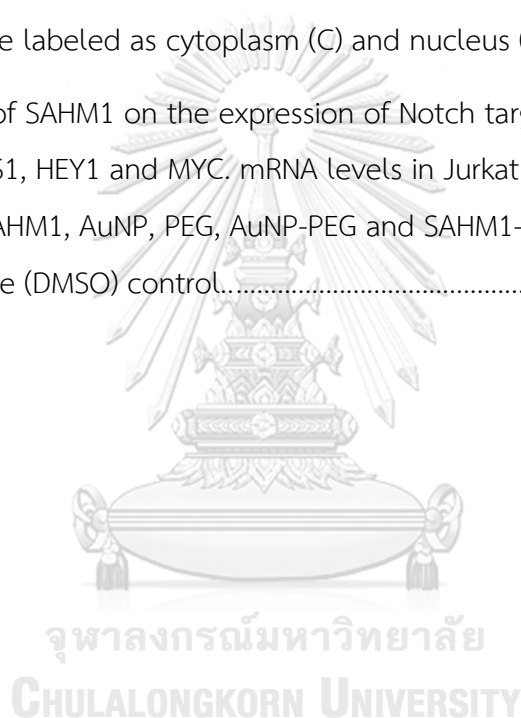
Figure 4.1 The absorbance values of SAHM1-PEG-AuNP conjugation. Solution color and the relation curve of SAHM1 concentration with respect to the absorbance at 520 nm. The result showed the minimal concentration of SAHM1 to stabilize the gold nanoparticle.....	34
Figure 4.2 UV-Visible spectrum of AuNP in size 40 nm and SAHM1-PEG-AuNP conjugate. Concentration of SAHM1-PEG-AuNP was 16.25, 31.30 and 62.50 μM of triplicate determination.....	35
Figure 4.3 TEM image (A) and frequency of particle size distribution graph (B) of AuNP (size 40 nm).....	36
Figure 4.4 TEM image (A) and frequency of particle size distribution (B) of AuNP-PEG.....	36
Figure 4.5 TEM image (A) and frequency of particle size distribution graph (B) of SAHM1-PEG-AuNP.....	37
Figure 4.6 Cytotoxicity of Jurkat cell line after treatment with SAHM1 (0-100 μM) for 24, 48 and 72 h.....	38
Figure 4.7 Morphology of Jurkat cell line after treatment with SAHM1. The image A, C and E were control (0.1% DMSO) and B, D and F were treated with 82.73, 65.67 and 17.54 μM of SAHM1 for 24, 48 and 72 h.....	39
Figure 4.8 Cytotoxicity of Jurkat cell line after treatment with DAPT. Concentrations of DAPT (0-100 μM) for 24, 48 and 72 h.....	40
Figure 4.9 Microscopic examination of Jurkat cell line after treatment for 24, 48 and 72 h. The image A, C and E were control (0.1% DMSO) and B, D and F were treated with 25, 54.56 and 20.22 μM of SAHM1.....	41
Figure 4.10 Cytotoxicity of AuNP in Jurkat cell line evaluated by MTT assay. %Cell viability after treatment of AuNP (0.001-1 μM) for 24, 48 and 72 h.....	42

Figure 4.11 Morphology and distribution of Jurkat cell line after treatment. The image A, C and E were control (sterile water) and B, D and F were treated with 40 nm of AuNP for 24, 48 and 72 h.....	43
Figure 4.12 Cytotoxicity of PEG in Jurkat cell line evaluated by MTT assay. %Cell viability after treatment with PEG (0-100 μ M) for 24, 48 and 72 h.	44
Figure 4.13 Microscopic examination of Jurkat cell line after treatment. The image A, C and E were control (0.1% DMSO) and B, D and F were treated with 100 μ M of PEG for 24, 48 and 72 h.	45
Figure 4.14 %Cell viability of Jurkat cell line after treatment with different reagents. Cytotoxicity of DAPT (50 μ M), SAHM1 (16.25 μ M), AuNP (16.25 μ M), PEG (16.25 μ M), AuNP-PEG (16.25 μ M) and SAHM1-PEG-AuNP conjugate for 24 and 48 h.	47
Figure 4.15 %Cell viability of Jurkat cell line after treatment with different reagents. Cytotoxicity of DAPT (50 μ M), SAHM1 (31.3 μ M), AuNP (31.3 μ M), PEG (31.3 μ M), AuNP-PEG (31.3 μ M) and SAHM1-PEG-AuNP conjugate for 24 and 48 ..	48
Figure 4.16 %Cell viability of Jurkat cell line after treatment with different reagents. Cytotoxicity of DAPT (50 μ M), SAHM1 (62.5 μ M), AuNP (62.5 μ M), PEG (62.5 μ M), AuNP-PEG (62.5 μ M) and SAHM1-PEG-AuNP (62.5 μ M) for 24 and 48 h.	49
Figure 4.17 TEM image of section in Jurkat cell line after incubation without AuNP (A and B) and treated with 31.3 μ M of SAHM1 (C and D) for 24 h. Low magnification of a whole cell section (A and C) and high magnification of part of cell section (B and D). Intracellular feature labeled as nucleus (N) and mitochondria (M).....	51
Figure 4.18 TEM image of Jurkat cell line after treatment with AuNP (31.3 μ M) for 24 h. Low magnification of a whole cell section (A and C) and high magnification of part of cell section (B and D). Red arrows marked AuNP, intracellular feature labeled as nucleus (N).....	52

Figure 4.19 Representative TEM images of section for Jurkat cell line after treatment with AuNP-PEG (31.3 μ M) for 24 h. Low magnification of a whole cell section (A and C) and high magnification of part of cell section (B and D). Red arrows marked AuNP, intracellular feature labeled as cytoplasm (C) and nucleus (N).....53

Figure 4.20 TEM images of Jurkat cell line after incubation with SAHM1-PEG-AuNP (31.3 μ M) for 24 h. Low magnification of a whole cell section (A and C) and high magnification of part of cell section (B and D). Red arrows marked AuNP, intracellular feature labeled as cytoplasm (C) and nucleus (N).54

Figure 4.21 Effect of SAHM1 on the expression of Notch target genes. qPCR analysis of the HES1, HEY1 and MYC. mRNA levels in Jurkat cell line treated for 48 h with DAPT, SAHM1, AuNP, PEG, AuNP-PEG and SAHM1-PEG-AuNP relative to dimethylsulphoxide (DMSO) control.....56



LIST OF ABBREVIATIONS

%	percent
°C	degree celsius
μl	microlitre
μM	micromolar
A	absorbance
AuNP	gold nanoparticle
ANOVA	Analysis of variance
BSA	bovine serum albumin
CO ₂	carbon dioxide
DAPT	N-[N-(3,5-Difluorophenacetyl)-L-alanyl]-S-phenylglycine t-butyl ester
DDI	double deionized water
DMSO	dimethyl sulfoxide
FCS	fetal calf serum
h	hour
IC50	50% inhibition concentration
λ_{max}	lambda max
M	molar
mg	milligram
min	minute
ml	millilitre
nm	nanometer
MTT	3-(4, 5-dimethylthiazol-2-yl)-2, 5 diphenyltetrasolium bromide
NaCl	sodium chloride
PBS	phosphate buffer saline
PEG	polyethylene glycol
rpm	round per minute
RPMI	Roswell Park Memorial Institute
SD	standard deviation

sec	second
SAHM1	stapled α -helical mastermind-like1
TEM	transmission electron microscopy
w/v	weight by volume



CHAPTER I

INTRODUCTION

1.1 Rationale

Cancer is a major cause of death affecting millions of people and is caused by the growth and spreading of abnormal cells in an uncontrolled manner. Currently, cancer treatment relies on surgery to remove cancer tissues and chemotherapy to destroy the remaining cancer cells and prevent reoccurrence. However, an alternative approach to cure cancer is based on specific target and the drug delivery system. Anticancer peptides (ACPs) have become promising molecules as novel anticancer agents. Stapled α -helical peptide from Mastermind-like 1 (SAHM1) has been reported to be specific anticancer peptide by inhibiting the Notch signaling pathway which is hyperactivated in various cancer cells including T cell leukemia. SAHM1 is a peptide mimicking Mastermind-like 1 protein and can interfere with the Notch signaling pathway. However, ACPs are susceptible to be digested by peptidase inside the target cancer cells. Therefore, a vector which can improve stability of the ACPs and safely transport the ACPs to the target cells is required for effective use by ACPs. In this research, thiol polyethylene glycol (thiol PEG) was linked to the gold nanoparticle (AuNP) for conjugation with SAHM1. AuNP was studied as the potential vector for molecular delivery of SAHM1 into Jurkat cell line, a human leukemia cancer cell line. AuNP have been used in a broad range of biological and biomedical applications due to their low toxicity. The cytotoxicity and localization of the SAHM1-PEG-gold nanoparticle conjugate (SAHM1-PEG-AuNP) in Jurkat cell line were investigated. In addition, the effect of the conjugate on activity of Notch signaling pathway was also studied. The results obtained from this study was beneficial to the development of SAHM1-PEG-AuNP as a new anticancer agent and/or may be used with the existing chemotherapeutic drugs for better therapeutic outcomes.

1.2 Objective of the Study

- To study cell penetration and localization of SAHM1-PEG-AuNP in Jurkat cell line
- To study the effect of SAHM1-PEG-AuNP on cell death of Jurkat cell line
- To study the effect of SAHM1 on Notch signaling pathway in Jurkat cell line

1.3 Scope of the Study

Study of SAHM1-PEG-AuNP conjugate was divided 4 parts; 1) preparation and characterization of SAHM1-PEG-AuNP conjugate. 2) cytotoxicity test of SAHM1-PEG-AuNP in Jurkat cell line. 3) internalization and localization of SAHM1-PEG-AuNP in Jurkat cell line. 4) activity of SAHM1-PEG-AuNP on Notch signaling pathway in Jurkat cell line.

1.4 Advantage of the Study

To approach target drug delivery for cancer treatment by application for gold nanoparticle as carrier for stapled SAHM1 peptide with target specific signaling pathway in cancer cells.

CHAPTER II

LITERATURE REVIEWS

2.1 Cancer

2.1.1 Causes of cancer

Cancer is a disease when cells divide abnormally without control (Figure 2.1) and can also spread to other parts of the body through the blood and lymph systems (Ferlay et al., 2010)

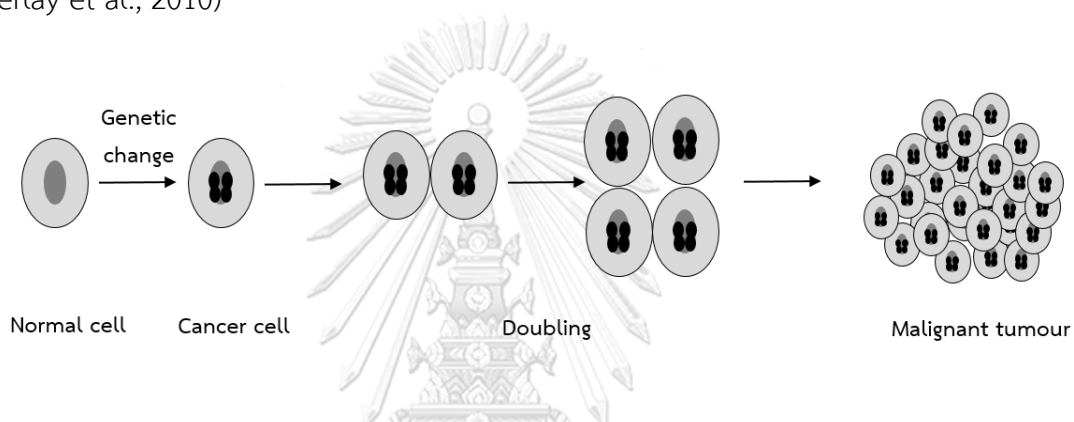


Figure 2.1 Development of normal cells to cancer cells.

Cancer is caused by accumulated damages to genes. Such changes may be due to change or to exposure to a cancer causing substance. The substances that cause cancer are called carcinogens. A carcinogen may be a chemical substance such as certain molecules in tobacco smoke. Cancer risk factors can be divided into following groups (Figure 2.2). First, biological factors (e.g. age, gender, inherited genetic defects and skin type). Second, environmental exposure (e.g. UV radiation). Then, occupational risk factors and carcinogens such as many chemical, radioactive materials and asbestos. After that, lifestyle-related factors (e.g. tobacco, alcohol and UV radiation in sunlight). Next, some food-related factors (e.g. nitrites and poly aromatic hydrocarbons generated by barbecuing food). Finally, bacteria and viruses such as *Helicobacter pylori*, which causes gastritis (Adam, 2003)

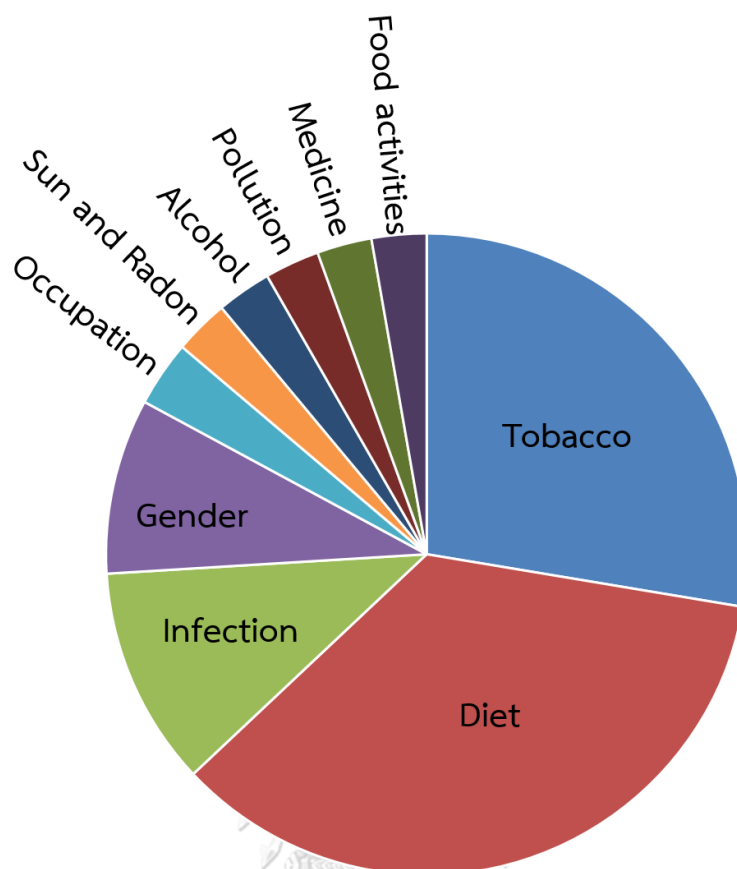


Figure 2.2 Risk factors of cancer. There are many types of risk factors of cancer. The most risk factors of cancer are tobacco, diet and infection.

จุฬาลงกรณ์มหาวิทยาลัย
CHULALONGKORN UNIVERSITY

2.1.2 Types of cancer

There are more than 100 types of cancer. Types of cancer name are usually called for the organs or tissues where the cancers form. Cancer may be discovered in different organs or tissues in body human. Figure 2.3 showed several types of cancer in worldwide. There are 5 main types of cancer. First, carcinoma is cancer that begins in the skin or in tissues that line or cover internal organs. There are different subtypes, including adenocarcinoma, basal cell carcinoma, squamous cell carcinoma and transitional cell carcinoma. Sarcoma is cancer that begins in the connective or supportive tissues such as bone, cartilage, fat, muscle or blood vessels. Leukemia is cancer that starts in blood forming tissue such as the bone marrow and causes

abnormal blood cells to be produced and go into the blood. Lymphoma and myeloma are cancers that begin in the cells of the immune system. Brain and spinal cord cancers are known as central nervous system cancers (Krentz et al., 2011).

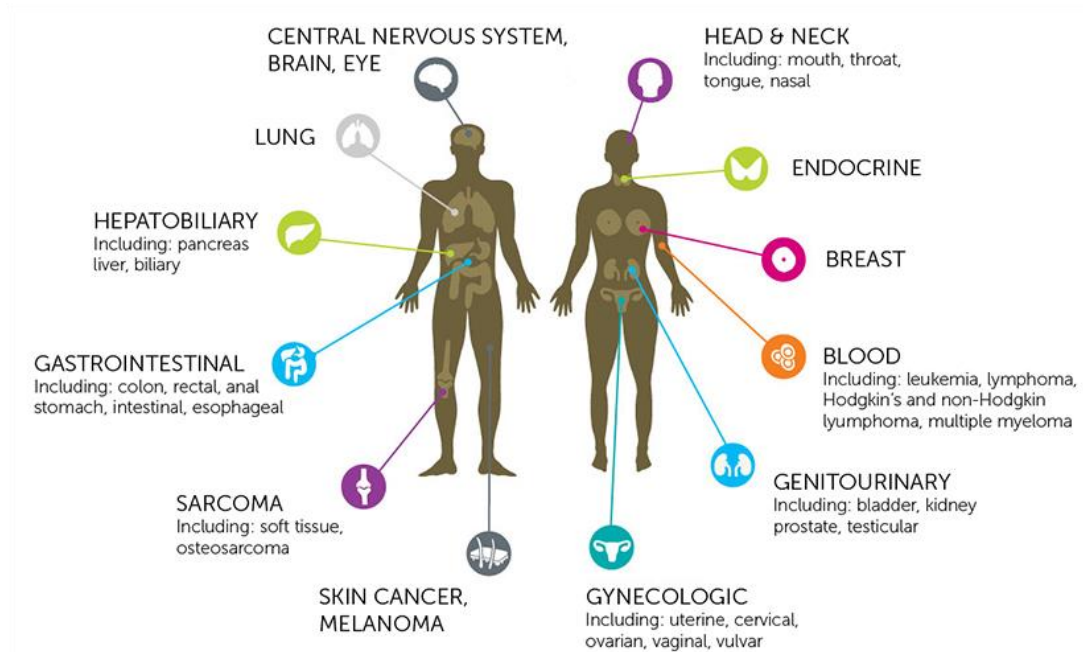


Figure 2.3 Cancer types of human worldwide. The types of cancer was depended on organ or tissue in human and called different name.

Available from: http://to15.onewalk.ca/site/PageServer?pagename=to15_aboutcancer
 [2018, January 10]

2.1.3 Cancer treatment

There are many types of cancer treatment. The types of treatment that the patient receives will depend on both type and stage of cancer. Some patients will have a combination of cancer treatments (Figure 2.4). The cancer treatments have limitation and side effects.

Surgery is a procedure in which a surgeon removes cancer from your body. Radiation therapy is a type of cancer treatment that uses high doses of radiation to kill cancer cells and shrink tumors (Parkin, 2006). Chemotherapy is a type of cancer

treatment that uses drugs to kill cancer cells. Immunotherapy helps immune system for fighting cancer cell. The immune system fights infections and other diseases in body. It is made up of white blood cells and organs and tissues of the lymph system.

Target therapy is a new type of cancer treatment that inhibit them grow, divide, and spread of cancer cell. Target therapy is combine radiation, surgery and chemotherapy (Figure 2.4). There are many substances for target therapy such as small-molecule drugs or monoclonal antibodies. Small-molecule drugs are small molecule vector such as anticancer peptides (ACPs) because it able to easily enter cell. The cell membrane of cancer cell attached with intracellular specific target cell for against cancer cell. Monoclonal antibodies attach specific target on the outer surface of cancer cells. Currently, small-molecule drugs or monoclonal antibodies conjugated with nanoparticle are used to inhibit a more specific target in cancer cell (Ahmad et al., 2001 and Nakanishi et al., 2001).

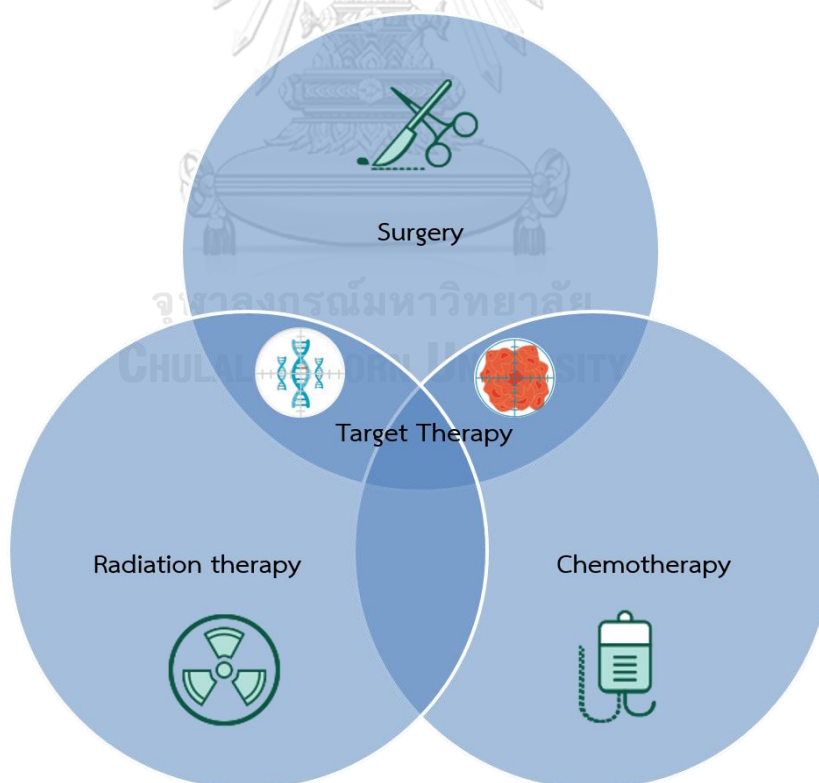


Figure 2.4 Cancer treatment from past to present. Target therapy is combined with radiation therapy, chemotherapy and surgery.

2.2 Leukemia

Leukemia is a cancer of the blood cells. There are several broad types of blood cells, including red blood cell (RBC), white blood cell (WBC), and platelet. Generally, leukemia refers to cancer type of the WBC. WBC is a vital part of immune system. It protects body from invasion by bacteria, fungi, and, viruses as well as from abnormal cells and other foreign substances. In leukemia, the WBC do not function like normal WBC. It can also divide too quickly and eventually crowd out normal cells. WBC is mostly produced in the bone marrow, but certain type of WBC is also made in the lymph nodes, spleen, and thymus gland. Once formed, WBC circulate throughout your body in your blood and lymph (fluid that circulates through the lymphatic system), concentrating in the lymph nodes and spleen (Aribi et al., 2007).

The causes of leukemia are not well known. However, many risk factors have been identified which may increase the risk. These include a family history of leukemia such as smoking and alcohol. Genetic and blood disorders such as down syndrome and myelodysplastic syndrome. Exposure of high levels of radiation and chemical such as benzene (Aribi et al., 2007).

Ray et al., 2010 reported that leukemia is also classified according to the type of cell. Leukemia involving myeloid cells is called myelogenous leukemia. Myeloid cells are immature blood cells that'd normally become granulocytes or monocytes. Leukemia involving lymphocytes is called lymphocytic leukemia. There are four main types of leukemia. They are acute myeloid leukemia (AML), acute lymphocytic leukemia (ALL), chronic myeloid leukemia (CML) and chronic lymphocytic leukemia (CLL) and show in Figure 2.5.

In 2012, National Cancer Institute (NIH) reported acute myeloid leukemia (AML) and acute lymphoblastic leukemia (ALL). In these diseases, the original acute leukemia cell goes on to form about a trillion more leukemia cells. These cells are described as nonfunctional because they do not work like normal cells. They also crowd out the normal cells in the marrow. This causes a decrease in the number of new normal cells made in the marrow. This further results in low red cell counts (anemia), low platelet counts (bleeding risk) and low neutrophil counts (infection risk).

Chronic myeloid leukemia (CML), the leukemia cell that starts this disease makes blood cells (red cells, white cells and platelets) that function almost like normal cells. The number of red cells is usually less than normal, resulting in anemia. But many white cells and sometimes many platelets are still made.

Chronic lymphocytic leukemia (CLL), the leukemia cell that starts this disease makes too many lymphocytes that do not function. These cells replace normal cells in the marrow and lymph nodes. They interfere with the work of normal lymphocytes, which weakens the patient's immune response. The high number of leukemia cells in the marrow may crowd out normal blood-forming cells and lead to a low red cell count (anemia). A very high number of leukemia cells building up in the marrow also can lead to low white cell (neutrophil) and platelet counts.

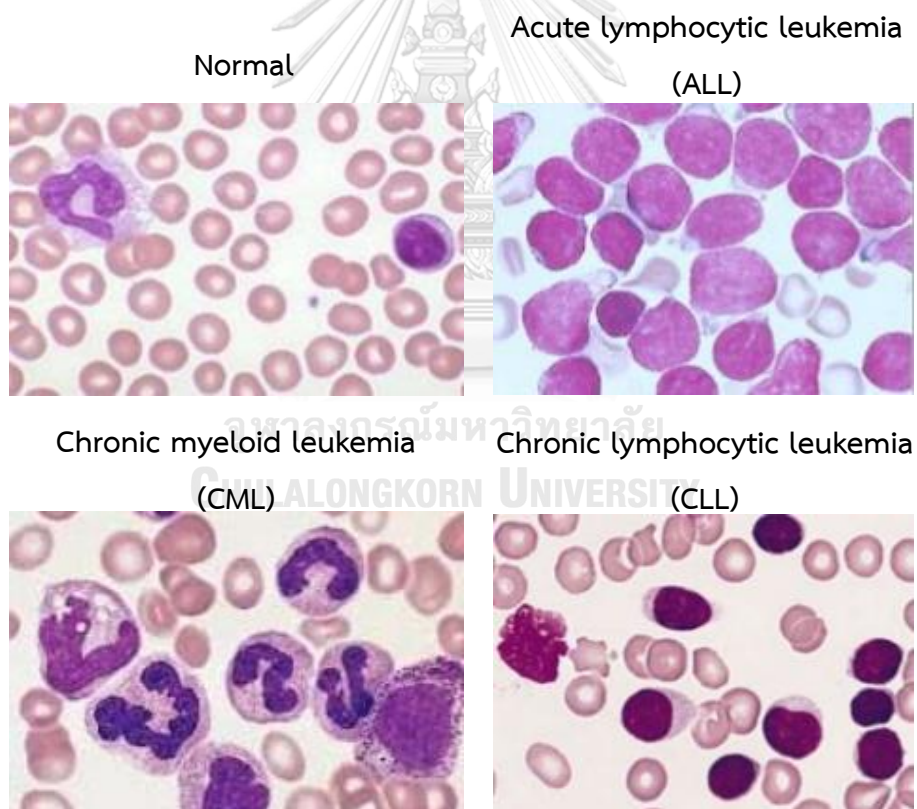


Figure 2.5 Morphology of abnormally white blood cell in leukemia. Diagnostics of leukemia was count white blood cell from blood (Hafez, Solaiman, Bilal, & Shalaby, 2016).

2.3 Stapled α -helical peptide of Mastermind-like 1 (SAHM1)

2.3.1 Notch signaling pathway

In Notch signaling pathway (Figure 2.6), binding of extracellular ligands to the Notch 1 receptor causes the proteolytic cleavage and release of the Notch 1 intracellular domain (NICD) (Moellering et al., 2009). Loss of the normal cellular restraints on Notch receptor processing and NICD stability in the nucleus leads to an inappropriate reactivation in Notch signaling in T cell acute lymphoblastic leukemia (T-ALL) and several other cancers. Notch signaling can be inhibited by chemical inhibitors of the γ -secretase complex (GSIs), which cleave the Notch1 receptor. However, chronic disruption of Notch signaling combined with off-target activities have limited the potential therapeutic use of these compounds and prompted a search for more selective inhibitors of the pathway (Jones, 2009).

A synthetic stapled 16 amino acids Mastermind-like1 (MAML1) peptide (SAHM1) binds to the preformed NICD-CSL complex and blocks recruitment of MAML1 to the Notch enhancer complex (Jones, 2009). Hydrocarbon-stapled α -helical peptide is a novel class of synthetic miniproteins locked into their bioactive α -helical fold through the site-specific introduction of a chemical brace (Figure 2.7). This prevents the expression of MAML1-dependent oncogenic Notch target genes. Notch or its signaling components are often mutated, resulting in uncontrolled cell proliferation (Verdine & Hilinski, 2012). Notch signaling can be inhibited with γ -secretase inhibitors, such as N-[N-(3,5-difluorophenacetyl-L-alanyl)]-(S)-phenylglycine t-butyl ester (DAPT). SAHM1, a peptide mimetic of a dominant negative form of MAML, inhibits canonical Notch transcription complex formation (Ashley, Ahn, & Hankenson, 2015).

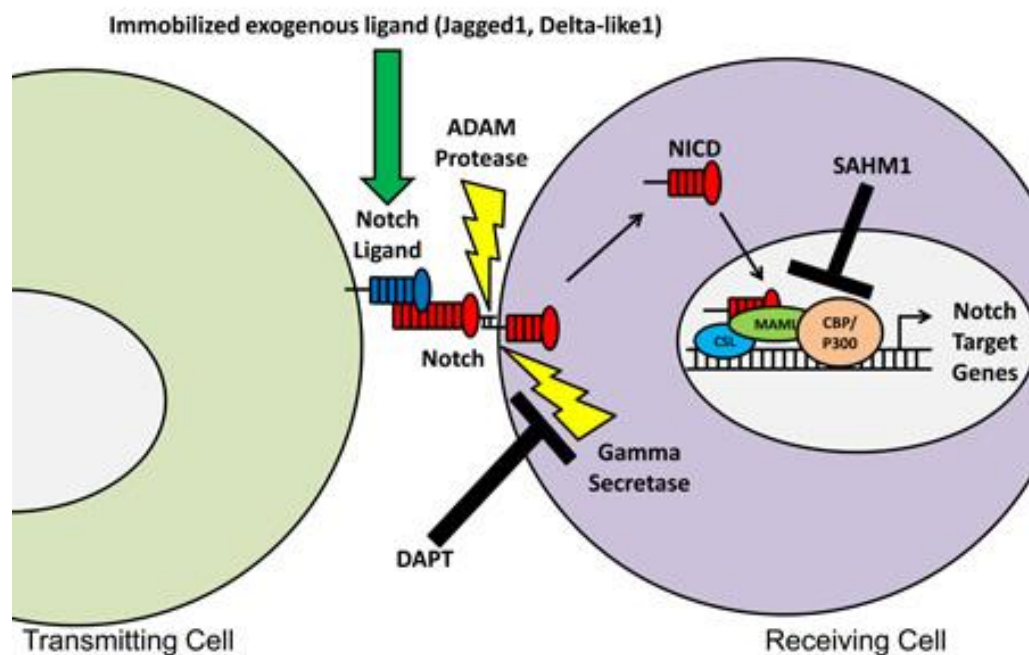


Figure 2.6 Experimental manipulation of Notch signaling pathway. Notch signaling was stimulated by plating cells on antibody-immobilized Fc-fusion proteins of either Jagged1 or Delta-like1. Notch signaling was inhibited with either the γ -secretase inhibitor, DAPT, which inhibits Notch signaling at the point of NICD release, or the dominant-negative MAML peptide mimetic, SAHM1, which inhibits Notch signaling at the transcriptional level; DMSO, the vehicle for both inhibitors, was used as the control for Notch inhibition (Ashley et al., 2015).

Figure 2.7 showed process of SAHM1 inhibiting the notch signaling pathway. Notch binds to other components in the cell and forms a complex that can turn on gene expression. Notice the yellow alpha-helix, which fits nicely in the complex for parts to activate gene expression. When the stapled peptide was attached with Notch complex, MAML1 cannot bind with Notch complex. Therefore gene expression cannot occur for inhibit Notch signaling pathway.

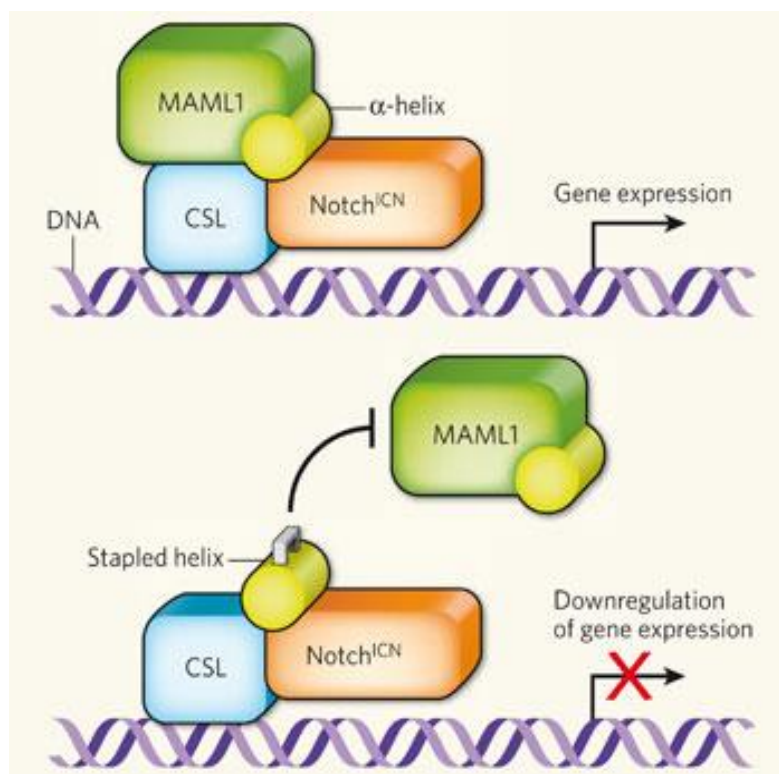


Figure 2.7 Process of SAHM1 inhibiting the Notch signaling pathway. Normally, CSL receptor was attached with MAML 1 form to activate Notch complex but SAHM1 was attached with Notch complex for inhibition of Notch signaling pathway (Mollering et al., 2010).

2.3.2 Design and synthesis of SAHM1

Stapled α -helical peptide of Mastermind-like 1 (SAHM1) was reported anticancer peptide. MAML1 is a co-activator protein to derive their design and potent dominant-negative inhibitor of oncogenic Notch signaling in T cell acute lymphoblastic leukemia (Moellering et al., 2009). The Notch signaling pathway is transiently induced during development to control cell proliferation and differentiation (Aster, Pear, & Blacklow, 2008).

The stapled peptides are protein fragments chemically locked into an α -helical shape (Figure 2.8). Helix stabilization by cross-linking had been shown previously to dramatically increase the helicity and potency of α -helical peptides. The stapled peptides can selectively target only one of a closely related family of proteins. They

are a promising class of alpha-helix mimetic inhibitors designed to be resistant to degradation, to penetrate cell membranes, and to bind tightly to disease target proteins. The stapled peptides can be used for intracellular drug targets because stapling can increase the target affinity and proteolytic resistance (Moellering et al., 2009). Amino acid sequence of SAHM1 was showed in Table 2.1. SAHM1 has both stapled α -helix cationic and amphipathic parts which enable the peptides to interact with the anionic molecules that are present in the membrane of cancer cells and disrupt the membrane integrity via several mechanisms.

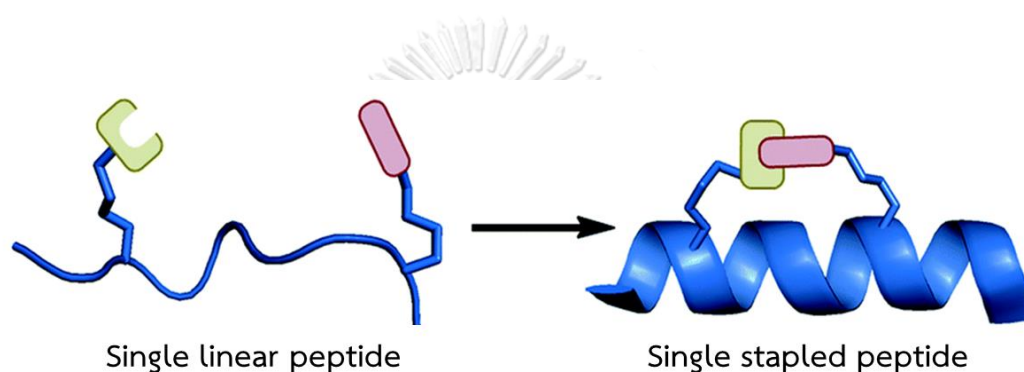


Figure 2.8 Structure of SAHM1 peptide. Amino acids were linked to linear peptide. Some amino acids were modified form to stapled peptide (Moellering et al., 2009).

Table 2.1 Sequences and helical character of MAML1-derived SAHM peptides.

Peptide	Sequence	Helicity (%)	Source protein	Target protein
MAML1	ERLRRREILCRRHHST	23	MAML	Notch
SAHM1	ERLRRR*ILCR*HHST	94	MAML	Notch/CSL

* S₅ non-natural alkenyl amino acid

Figure 2.9 showed design of MAML1-derived stapled peptides targeting Notch-CSL complex structure of the Notch ternary complex (Protein Data Bank (PDB) accession 2F8X). A kinked α -helix from the MAML transcriptional coactivator protein binds to a cleft created by the Notch/CSL complex. The α -carbons of the MAML

residues not expected to interact with the Notch/CSL complex are shown as spheres. The region of MAML from which the bioactive SAHM1 stapled peptide was designed is indicated with a box. MAML residues E28 and R32 were replaced with non-natural alkenyl amino acid (S5) cross-linking amino acids to form SAHM1 (Verdine & Hilinski, 2012). Residues 16–70 of the MAML coactivator protein are shown, along with the sequence of the SAHM1 stapled peptide. Residues in red appear to contact the Notch/CSL complex, whereas residues in black do not appear to be involved in the interface. Residues 45 and 46 of the MAML protein (shaded gray) correspond to the kink in the MAML α -helix (Moellering et al., 2009). Molecular structure of SAHM1 peptide was showed in Figure 2.10.

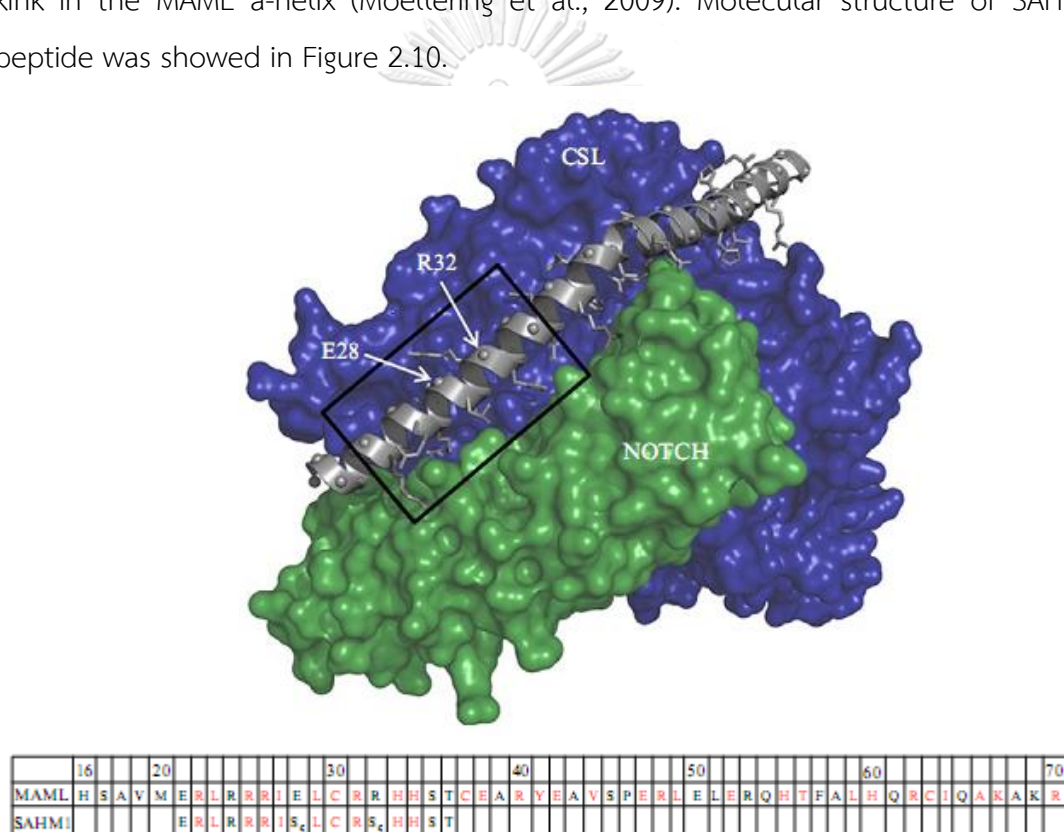


Figure 2.9 Design of stapled peptides targeting the Notch/CSL complex. SAHM1 was modified from MAML1 of Notch complex (Verdine & Hilinski, 2012).

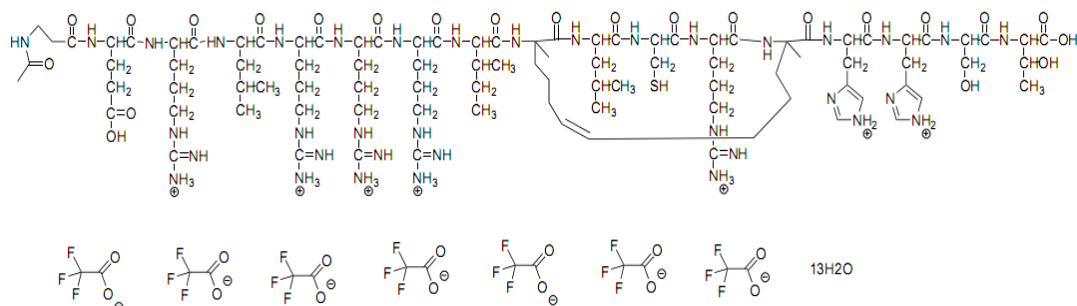


Figure 2.10 Molecular structure of SAHM1 peptide. SAHM1 molecule was consisted of $C_{94}H_{162}N_{36}O_{23}S \cdot 7CF_3CO_2 \cdot 13H_2O$ (Moellering et al., 2009).

2.3.3 Functions of SAHM1

Figure 2.11 showed several functions of SAHM1. Stapled peptide was penetrated, specific and staple into target cell. Stapling can greatly improve the pharmacologic performance of peptides, increasing target affinity, proteolytic resistance, and serum half-life while conferring on them high levels of cell penetration.

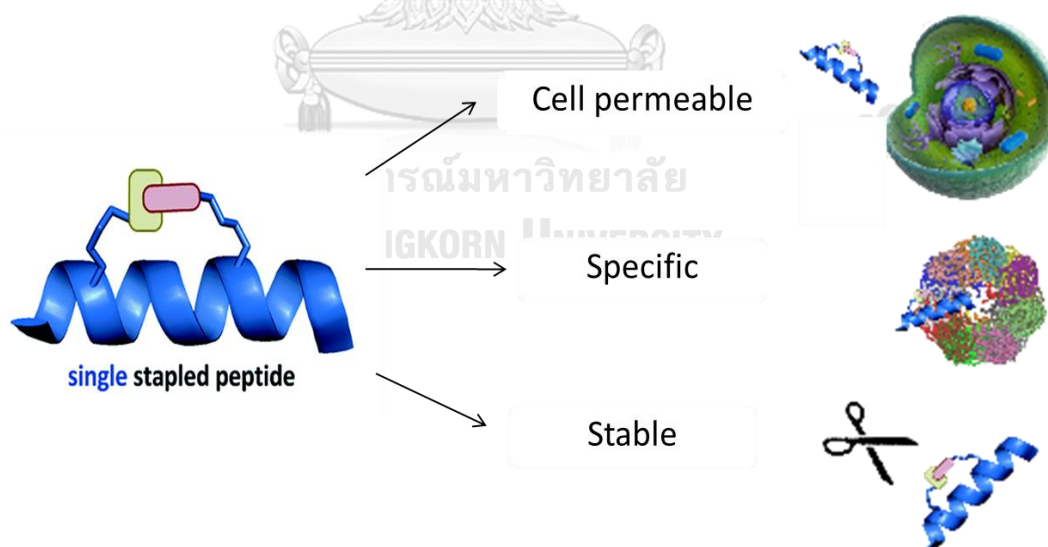


Figure 2.11 Functions of stapled peptide. The stapled peptides can be used for intracellular drug targets because stapling can increase the target affinity and proteolytic resistance.

2.3.4 Stapled peptide in cancer therapy

Bradner et al., 2009 became deeply interested in a human protein called Notch. The gene encoding this protein is often damaged, or mutated, in patients with a form of blood cancer, known as T-cell acute lymphoblastic leukemia (T-ALL). Abnormal Notch genes found in cancer patients remain in a state of constant activity, switched on all the time, which helps to drive the uncontrolled cell growth that fuels tumors. Similar abnormalities in Notch also underlie a variety of other cancers, including lung, ovarian, pancreatic and gastrointestinal cancers.

Verdine et al., 2010 invented a drug discovery technology that uses chemical braces or "staples" to hold the shapes of different protein snippets. Without these braces, the snippets (called "peptides") would flop around, losing their three-dimensional structure and thus their biological activity. Importantly, cells can readily absorb stapled peptides, which are significantly smaller than proteins. That means the peptides can get to the right locations inside cells to alter gene regulation. After designing and testing several synthetic stapled peptides, the research team identified one with remarkable activity. Not only could it bind to the right proteins and reach the right places inside cells, it also showed the desired biological effect: the ability to disrupt Notch function.

2.4 Gold nanoparticle

2.4.1 History of nanoparticle

Nanotechnology, a newly evolved discipline includes the formation, management and application of structures in the nanometer size range (Athar & Das, 2013). It has the great potential to transform different fields including pharmacy and medicine. Many nanomaterials like nanotubes, nanoshells, nanorods and nanoparticles are mostly used as a part of nanomedicine. Nanotechnology provides new tools for the molecular treatment of several diseases and its rapid detection. It advances materials with a nanometric dimension and provides several means for innovative design of size of nanoparticle for drug delivery systems to overcome biological barriers in order to direct the drug (Brandelli, 2012; Wang et al., 2010).

In general, the size of a nanoparticle is between 1 to 100 nm. Metallic nanoparticles have different physical and chemical properties such as lower melting points, higher specific surface areas, specific optical properties, mechanical strengths, strong adsorption and specific magnetizations (Horikoshi & Serpone, 2013). However, usage of nanoparticle is depended on the specific application.

Boogaard et al., 2009 reported that many drugs and therapies are made available to counteract most fatal illnesses like AIDS, cancer, tuberculosis and cardiovascular diseases. Athar and Das (2013) reported that nanoparticles specifically noble metal nanoparticle, generally use biological pathways to achieve drug delivery to cellular and intracellular targets, including transport through the blood–brain barrier.

2.4.2 Applications of gold nanoparticle in biological and medical

Gold nanoparticle (AuNP) has been used in a broad range of biological and biomedical applications such as chemotherapy, cancer therapy, imaging, water remediation, biosensors and drug delivery etc (Park, Tsutsumi, & Mihara, 2013). Because they are noncytotoxic and easy to be synthesized, have high solubility and excellent light scattering property.

More recently, these unique optical-electronics properties have been researched and utilized in high technology applications. The range of AuNP applications is growing rapidly and includes microelectronics (chips, sensors and probes), biomedical applications, and catalysis (Daniel & Astruc, 2004). AuNP is being used as conductors, connect resistors, and other elements of electronic chips, in a variety of sensors (Jakobs et al., 2008; Zhao, Zhong, Kim, Liu, & Liu, 2014) and as useful probes for imaging applications (He, Xie, & Ren, 2008). Biomedical applications of AuNP is also increasing, as drug delivery agents, for diagnosis of heart diseases, cancers and infectious agents, and in cancer therapy (Boisselier & Astruc, 2009; Dykman & Khlebtsov, 2011; Jain, Hirst, & O'Sullivan, 2012).

Table 2.2 showed important biomedical applications summaries of gold nanoparticle. AuNP has many advantages in biomedical as drug delivery carriers, their size generally prevents them from attaching the plasma membrane.

Table 2.2 Examples of biomedical applications of gold nanoparticle.

Type of gold nanoparticle	Biomedical applications	References
AuNP	Cancer detection	(Hainfeld et al., 2010)
AuNP	Drug delivery	(Patra, Bhattacharya, Mukhopadhyay, & Mukherjee, 2010)
Dendrimer-entrapped AuNP	Imaging	(Wang et al., 2012)
Gold-coated Au@tiopronin NP	Cancer treatment	(Huo et al., 2013)
Fluorescein-labeled oligomannoside AuNP	HIV treatment	(Arnaiz, Martinez-Avila, Falcon-Perez, & Penades, 2012)
Glucose-coated AuNP		(Chiodo, Marradi, Calvo, Yuste, & Penades, 2014)
AuNP	Biomedicine (biomedical applications)	(Cabuzu, Cirja, Puiu, & Grumezescu, 2015; Zhang, 2015)
AuNP	Imaging, drug delivery, tissue engineering, etc.	(Kim, Kumar, Khanga, & Lim, 2015)

2.4.3 Synthesis of gold nanoparticle

Colloidal gold nanoparticle is produced by reduction of tetrachloroauric acid (HAuCl_4) and sodium borohydride (NaBH_4). The most common method developed from Turkevich method (Kimling et al., 2006). The catalytic reduction of tetrachloroauric acid (HAuCl_4) is used by sodium borohydride in water (H_2O). Sodium borohydride is reducing agent and capping agent for coated surface of gold nanoparticle. The following reaction shows a chemical reduction reaction (Figure 2.12).



Figure 2.13 showed synthesis of gold nanoparticle method. Briefly, the tetrachloroauric solution is boiled and stirred on hot plate stirrer. After that, sodium borohydride is added as the reducing agent and capping agent. Immediately, the Au^{3+} ions is reduced to neutral gold atoms and start to form in the solution and their concentration rises rapidly until the solution reaches supersaturation. Aggregation subsequently occurs in a processed called nucleation, with central icosahedral gold cores of 11 atoms forming at nucleation sites. This nucleation process occurs very quickly. Once it is achieved, the remaining dissolved gold atoms continue to bind to the nucleation sites until all atoms are removed from solution (Kimling et al., 2006).

The particle size in the suspensions is determined by the number of nuclei over which the available gold is divided and is not a result of the reduction of a different percentage of the available gold. Thus, the more the nuclei, the smaller the gold particles would be produced. The number of nuclei is depended on the amount of the ions. Therefore, to produce larger particles, less sodium borohydride should be added (Frens, 1973).

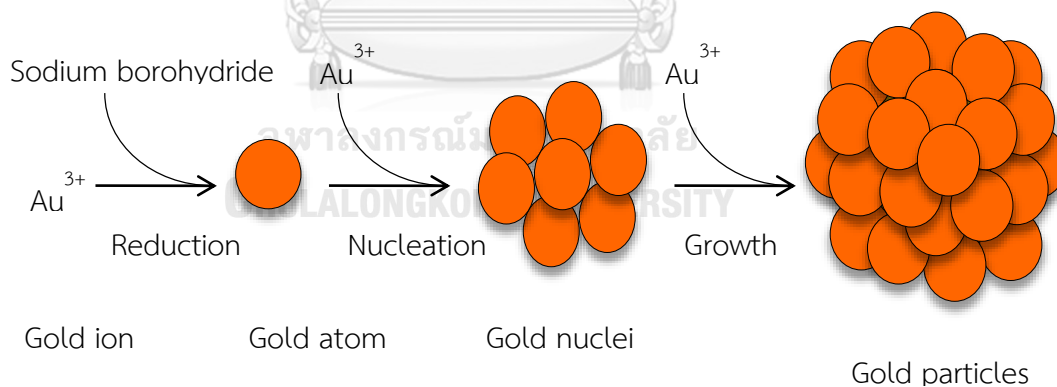


Figure 2.12 Formation of gold nanoparticle by the sodium borohydride capping. The Au^{3+} ions is reduced to neutral gold atoms and start to form in the solution.

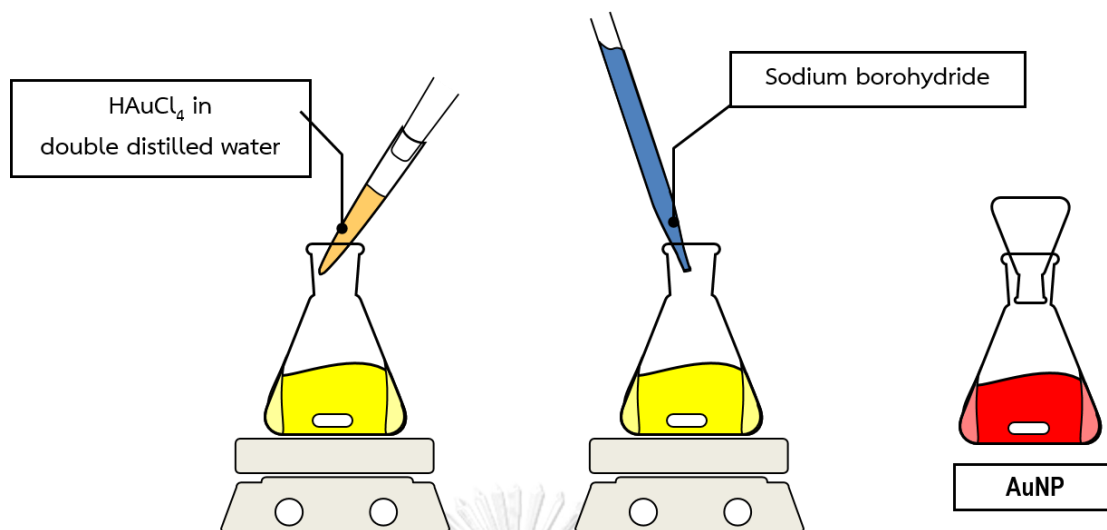


Figure 2.13 Synthesis of gold nanoparticle by Turkevich method. Gold nanoparticle is produced by reduction of tetrachloroauric acid (HAuCl₄) by using sodium borohydride (NaBH₄) for reducing agent and capping agent.

2.4.4 Method of conjugation protein and peptide to gold nanoparticle

The aim is to use gold nanoparticle (AuNP) in biomedicine as diagnostic and therapeutic agents in cells or tissues. It is necessary to rightly choose the targeting component such as a peptide, monoclonal antibody, and the strategy to attach it on the surface of the particle. AuNP conjugated by peptide or other functionalized groups have also been used as effective agents for diagnostic and therapeutic applications (Cao-Milan & Liz-Marzan, 2014).

The method for attaching peptide and other molecules to AuNP surface are divided 2 parts, it was physical and chemical interactions (Figure 2.11).

Physical Interaction between peptide and AuNP depends on three phenomena: (a) ionic attraction between the negatively charged gold and the positively charged antibody; (b) hydrophobic attraction between the antibody and the gold surface; (c) dative binding between the gold conducting electrons and amino acid sulfur atoms of the antibody (Ljungblad, 2009).

Chemical interactions between peptides and nanoparticle surface are achieved in the number of ways like (a) chemisorption via thiol derivatives; (b) through the use

of bifunctional linkers (c), and through the use of adapter molecules (Jazayeri, Amani, Pourfatollah, Pazoki-Toroudi, & Sedighimoghaddam, 2016).

Thiolated polyethylene glycol (PEG-SH) is used to coat bare AuNP surfaces to decrease nonspecific interactions. The hydrophilic nature of PEG also increases the biocompatibility of the conjugate. The PEGylated AuNP used were carboxyl terminated, providing a chemical group suitable for covalent binding. Although carboxyl groups do not spontaneously form bonds to antibodies, they can be chemically modified to serve this purpose (Zhou, Andersson, Lindberg, & Liedberg, 2004).

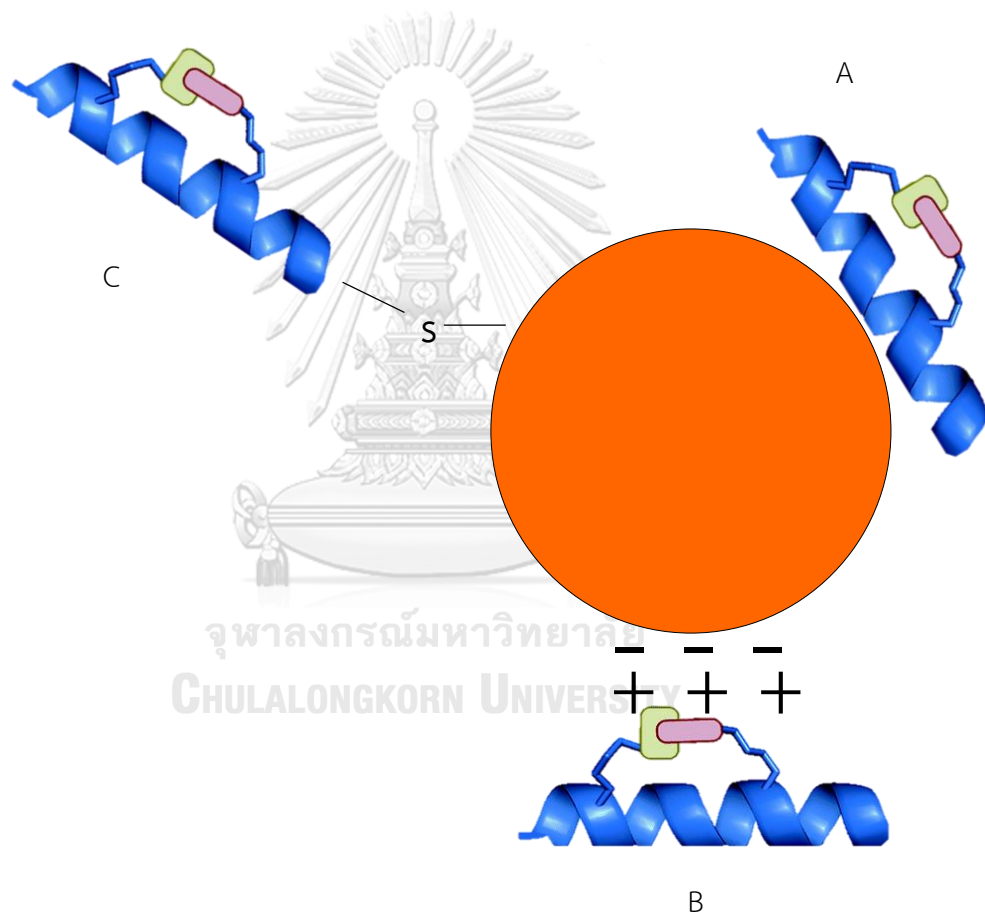


Figure 2.14 Hydrophobic and ionic interactions between peptide (blue) and gold nanoparticle surface (orange). A) Hydrophobic interaction B) ionic interaction C) a covalent bond is formed due to dative binding.

2.5 Jurkat cell line

Jurkat cell lines are an immortalized line of acute T lymphocyte cells that are widely used to study acute T cell leukemia, T cell signaling, and the expression of various chemokine receptors (Schneider, Schwenk, & Bornkamm, 1977).

Jurkat cell lines are spherical in shape and usually grow in suspension without adherent to a surface (Figure 2.15). Jurkat cell line was established from peripheral blood of 14 years old boy.

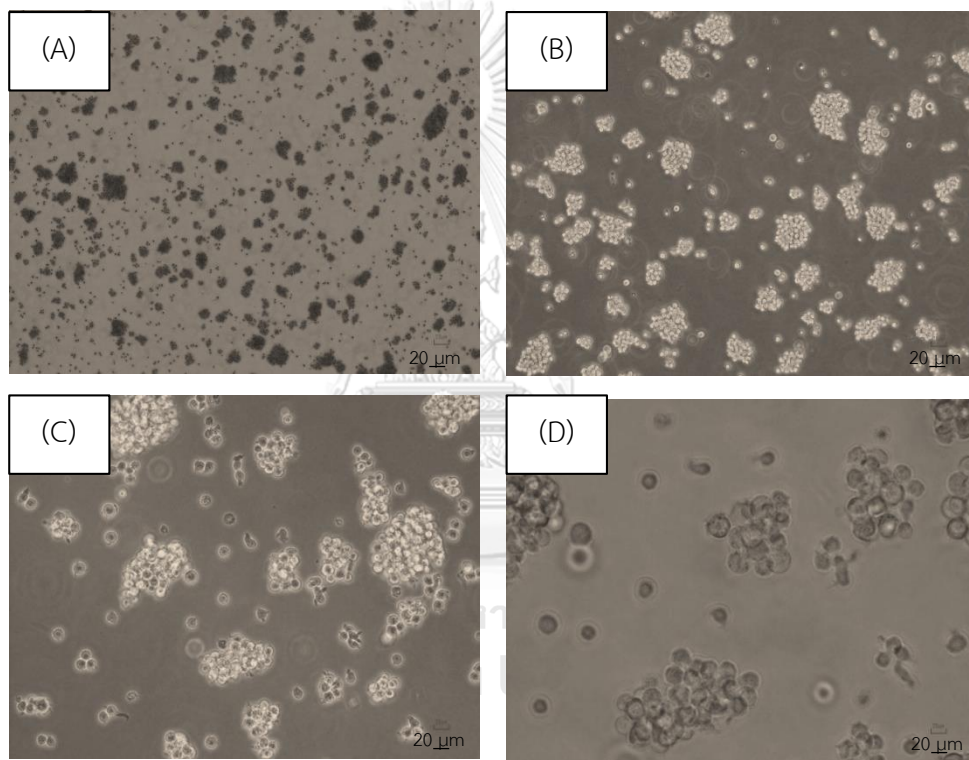


Figure 2.15 Morphology of Jurkat cell line. All images were magnified 40X (A), 100X (B), 200X (C) and 400x (D) and the scale bar was 20 μm.

CHAPTER III

MATERIALS AND METHODS

3.1 Chemicals and reagents

- Colloidal gold nanoparticle Kestrel Biosciences Co., Ltd. ,
Pathumthani, Thailand
- Dimethyl sulfoxide (DMSO) Sigma-Aldrich, St. Louis, USA
- Diphenyltetrazolium bromide Bio Basic, New york, USA
(MTT)
- Di-sodium hydrogen phosphate Merck, Darmstadt, Germany
(Na_2HPO_4)
- Ethanol Merck, Darmstadt, Germany
- Fetal calf serum (FCS) Hyclone, GE Healthcare life
Science, USA
- Glucose Sigma-Aldrich, Missouri, USA
- Glutaraldehyde Sigma-Aldrich, Missouri, USA
- L-glutamine Sigma-Aldrich, Missouri, USA
- Monopotassium phosphate (KH_2PO_4) Sigma-Aldrich, Missouri, USA
- N-[N-(3,5-Difluorophenacetyl)-L-alanyl]- EMD Millipore, Billerica, USA
S-phenylglycine t-butyl Ester (DAPT)
- Osmium tetroxide (OsO_4) Sigma-Aldrich, Missouri, USA
- Poly (ethylene glycol) methyl ether SynQuest, SynQuest laboratories,
thiol, Mn5000 USA
- Potassium chloride (KCl) Sigma-Aldrich, Missouri, USA
- Roswell Park Memorial Institute medium Biochrom, Berlin, Germany
(RPMI-1640)
- SAHM1 EMD Millipore, Billerica, USA
- Sodium bicarbonate (NaHCO_3) Sigma-Aldrich, Missouri, USA

- Sodium carbonate (Na_2CO_3) Merck, Darmstadt, Germany
- Sodium chloride (NaCl) Merck, Darmstadt, Germany
- Sodium pyruvate ($\text{C}_3\text{H}_3\text{O}_3\text{Na}$) Sigma-Aldrich, Missouri, USA

3.2 Equipments

- -20°C Freezer Sanyo, Chachoeng Sao, Thailand
- -70°C Freezer Sanyo, Osaka, Japan
- 37°C, 5%CO₂ Incubator Yamato, Tokyo, Japan
- 4°C Refrigerator Toshiba, Nonthaburi, Thailand
- 6, 24 and 96-well culture plate Corning, New York, New York
- Autoclave Udono, Tokyo, Japan
- Autopipette tip, 10, 100, 300 and 1000 Axygen, Union City, California
- Autopipette, P10, P20, P200 and P1000 Eppendorf, Hamburg, Germany
- Biological Stirrer, 2 Position Techne, Staffordshire, UK
- Centrifuge tube, 15 and 50 ml Axygen, Union City, California
- Centrifuge, model: universal 320, swing out rotor 1619 Hettich, Tuttlingen, Germany
- Cryotube, 2 ml Nunc, Roskilde, Denmark
- Disposable syringe, 5 ml and 10 ml Nipro, Autthaya, Thailand
- Examination gloves Magaglove, Chon Buri, Thailand
- Filter paper #1 Whatman, Kent, UK
- High speed refrigerator centrifuge, model: 6500, rotor AG-508CA Kubota, Tokyo, Japan
- Hot plate stirrer, model: C-MAGHS7 IKA Work, Wilmington, North Carolina 39
- Industrial N₂ gas Linde, Samut Prakan, Thailand
- Inverted microscope, model TMS Nikon, Tokyo, Japan

- Laminar flow Lab Survice Ltd., Bangkok, Thailand
- Liquid Nitrogen Tank Harsco Corp., Camp Hill, Pennsylvania
- Microcentrifuge tube, 1.5 ml Axygen, Union City, California
- Microplate reader, model: MCC/340 Titertek multiskan, Helsinki, Finland
- Multichannel autopipette HTL, Warsaw, Poland
- Multi-detection microplate reader, Synergy HT BIO-TEK, Richmond, Virginia
- NanoDrop spectrophotometer Thermo Scientific, Virginia, USA
- Orbital shaker Fisher Scientific, Illkirch-Graffenstadam, France
- Petri dish, 60 and 90 mm Sterilin Ltd., Newport, UK
- pH Meter, model: AB15 Fisher Scientific, UE Tech Park, Singapore
- Pipettes, 10 ml HBG, Luetzelinden, Germany
- Real-time PCR Bio-Rad laboratories, California, USA
- Syringe filter, Nylon membrane, 0.45 μm , 13 mm Whatman, Kent, UK
- T Flask Corning, New York, New York
- Transmission electron microscopy (TEM) JEM 1400, JEOL, Japan
- Vacuum pump Iwaki pump, Fukushima, Japan
- Vortex mixer Scientific Industries, Boulder, Colorado
- Water bath Memmert, Schwabach, Germany

3.3 Experimental procedures

Part I Preparation of SAHM1-PEG -gold nanoparticle conjugate

3.3.1 Optimization of SAHM1 peptide for conjugate on gold nanoparticle

Solution of colloidal gold nanoparticle (40 nm) was adjusted to pH 9.0 with 0.2 M of Na_2CO_3 . SAHM1 peptide (7.25 μl) was diluted in the range 0-250 μM in dimethyl sulfoxide (DMSO) and mixed 7.25 μl with poly (ethylene glycol) methyl ether (PEG). Then, the mixture was added 10 μl into 96 well plate. Colloidal gold nanoparticle (100 μl) was added into each well, the plate was incubated at room temperature for 1 hr. Finally, 80 μl of 10% NaCl was added to precipitate the gold nanoparticle. The absorbance at 520 nm was measured. The optimum concentration of the SAHM1 peptide was the least concentration that yields the highest absorbance.

3.3.2 Conjugation of SAHM1-PEG-gold nanoparticle

The method of preparation and characterization of SAHM1-PEG-gold nanoparticle conjugate (SAHM1-PEG-AuNP) was modified from Park et al., 2013 and Tkachenko et al., 2005. The formation of SAHM1-PEG-AuNP was showed in Figure 3.1. Combine 72.5 μl of thiol PEG (31.25 μM) and 72.5 μl of SAHM1 peptide (31.25 μM) to produce a molar ratio of thiol PEG to SAHM1 peptide of 1:1. Solution of colloidal gold nanoparticle (40 nm) was adjusted to pH 9.0 with 0.2 M of Na_2CO_3 . After that, colloidal gold nanoparticle (100 μM) was added 1 ml into the mixture. Then, the mixture was shaken and stirred at room temperature for 1 h to allow complete exchange of thiol with citrate on the gold nanoparticle. The complex was washed by centrifugation at 12,000 rpm for 30 min and resuspended with 1 ml of double deionized water (DDI). SAHM1-PEG-AuNP sample was characterized by UV-VIS spectroscopy at 400 to 800 nm wavelengths (Figure 3.2). In addition, the sample was observed by transmission electron microscopy (TEM) to check for shape and size of the particle and determined size distribution of the particle by Image J analysis.

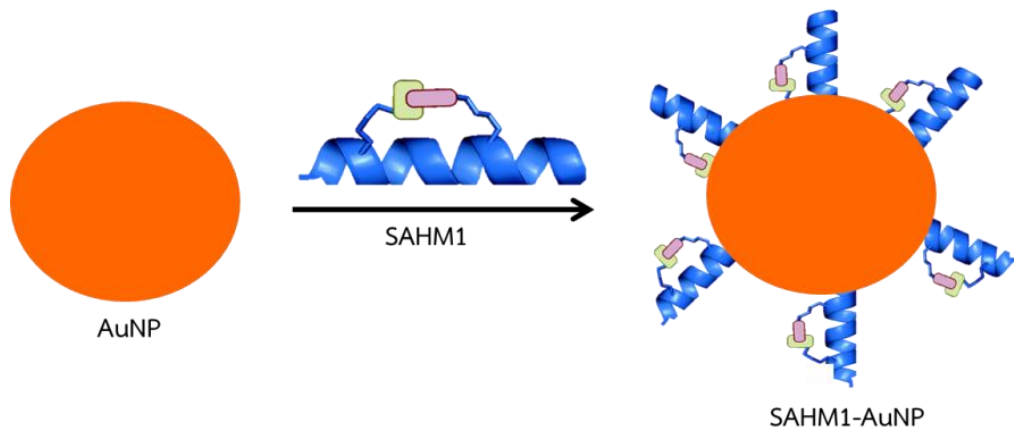


Figure 3.1 Predicted formation of SAHM1-gold nanoparticle conjugate.

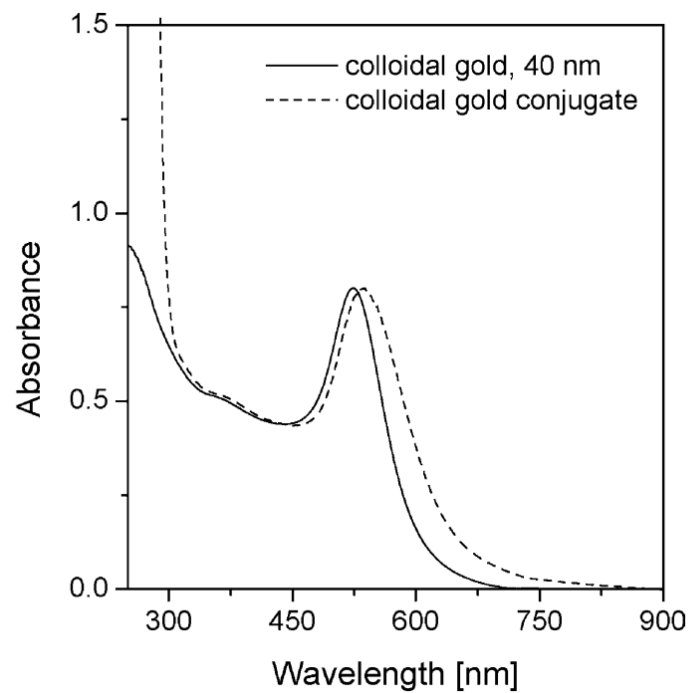


Figure 3.2 Shift in surface plasmon absorption of AuNP (40 nm) due to protein conjugation. Both spectra were normalized to the maximum of the plasmon band (Seydack, 2005).

Part II Cytotoxicity of SAHM1-PEG-AuNP

3.3.3 Cell culture

Jurkat cell line was obtained from American Type Culture Collection (ATCC TIB-152). Jurkat cell line was cultured in Roswell Park Memorial Institute medium (RPMI-1640) with supplemented with 10% (v/v) fetal calf serum (FCS), 10 U/ml penicillin, 0.4 mg/ml streptomycin and 1% (w/v) sodium pyruvate.

3.3.4 Cytotoxicity assay

Cytotoxicity test was performed by standard MTT assay. The colorimetric MTT test assesses cell metabolic activity based on the ability of the mitochondrial succinate/tetrazolium reductase system to convert the yellow dye (MTT) to a purple formazan in living cells (Figure 3.3). The metabolic activity of the cell is proportional to the color density formed. (Liu et al., 2013)

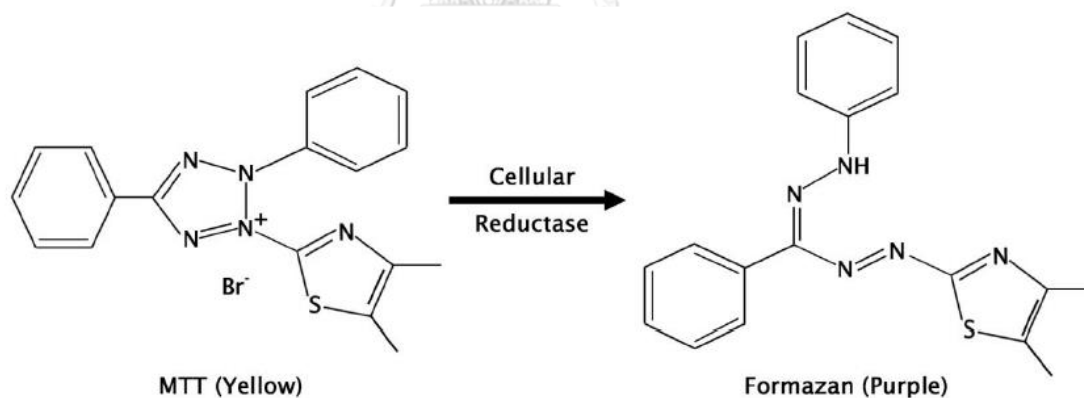


Figure 3.3 Chemical structure of the yellow dye (MTT) and the converted to a purple formazan in living cells (Yamaori et al., 2013).

Jurkat cell line was seeded in 96 well plate at certain density (5×10^4 cells per well) and incubated for 24 h at 37°C under 5% CO_2 . Then, SAHM1, DAPT and PEG were dissolved in DMSO for final concentration of 0-100 μM and added in each well. For control, the use of 0.1% of DMSO was performed. For solution of colloidal AuNP (40 nm, 100 μM) was centrifuged at 12,000 rpm, 4°C for 30 minutes to separate the particles. The pellet of capped AuNP was washed with double distilled water (DDI) and centrifuged two times again to remove excess chemical for further use. Before treatment, the AuNP solution was filtered by column (0.2 μM) for protect contamination. For the conjugate, AuNP-PEG and SAHM1-PEG-AuNP were added in each well. After that, the plate was incubated for 24, 48 and 72 h at 37°C under 5% CO_2 . Cytotoxicity test was examined by MTT assay. MTT solution (5 mg/ml) was added 10 μl per well. Next, the plate was centrifuged at 1,500 rpm for 15 minutes and incubated for 4 h at 37°C under 5% CO_2 . The MTT solution was removed and 150 μl of DMSO was added to each well. The optical density was detected using microplate reader at 540 nm wavelength. The mean absorbance of the control wells represented 100% cell survival by three repeat experiments. The mean inhibitory concentration (IC_{50}) representing the concentration at which cell viability was reduced by 50% (Figure 3.4). The percentage of cell viability was calculated according to the following formular.

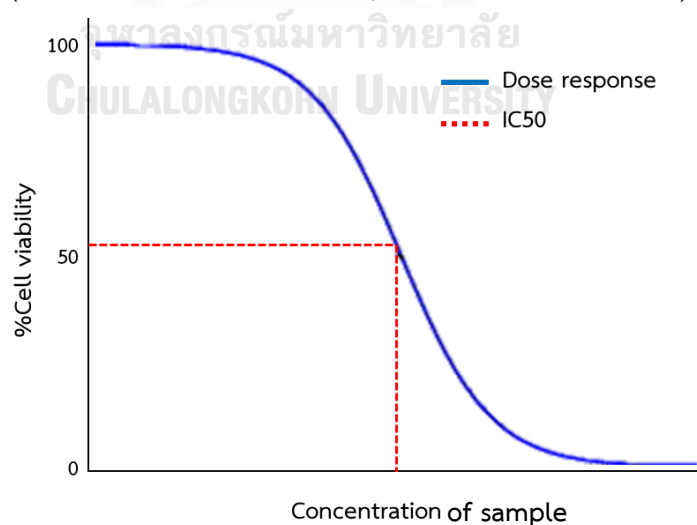
$$\% \text{cell viability} = (\text{absorbance of treated cells} / \text{absorbance of control}) \times 100$$


Figure 3.4 Example of inhibitory concentration (IC_{50}) curve.

Part III Internalization and localization of SAHM1-PEG-AuNP in cells

For transmission electron microscopy (TEM) cell section analysis, Jurkat cell line was seeded in 6 well plate at a density of 1×10^6 cells per well and incubated for 24 h at 37°C under 5% CO₂. After that, SAHM1 (31.3 μM), 40 nm of AuNP (31.3 μM), AuNP-PEG (31.3 μM) and SAHM1-PEG-AuNP (31.3 μM) were added 50 μl in each well and incubated for 24 h at 37°C under 5% CO₂. The untreated cell was used as the control. At a determined time, the cells were washed three times with PBS, centrifuged at 1,500 rpm, 5 min, 25°C and fixed with 2.5% glutaraldehyde in 0.1 M phosphate buffer. After 2 h, the cells of fixation at 4°C, the samples were washed with phosphate buffer saline (0.1 M, pH 7) three times. Then, the samples were fixed with 1% osmium tetroxide in 0.1 M phosphate buffer for 2 h at 4°C. After being washed in water, the samples were dehydrated in alcohol series, embedded, and sliced with the thickness between 60 and 90 nm. The samples were observed by transmission electron microscopy (TEM) to check the internalization and localization of SAHM1-PEG-AuNP in cells at Scientific and Technological Research Equipment Center (STREC), Institute Building 2, Chulalongkorn University.

Part IV Effect of SAHM1-AuNP on Notch signaling pathway

3.3.7 Cell culture

Jurkat cell line was seeded in 6 well plate at certain density (1×10^6 cells per well) and incubated for 24 h at 37°C under 5% CO₂. SAHM1 (31.3 μM), 40 nm of AuNP (31.3 μM), AuNP-PEG and SAHM1-PEG-AuNP (31.3 μM) were added in each well. For positive control, the use of DAPT (50 μM) was performed and the untreated cell was used as the negative control. The plate was incubated for 24 h at 37°C under 5% CO₂.

3.3.8 RNA extraction and quantitative RT-PCR

To isolate RNA was followed by Trizol lysate protocol was followed Invitrogen, Thermo Scientific. Trizol reagent (500 μl) was added to cells. Chloroform was added 100 μl to each sample and vigorously shaken for 15 sec. Samples were centrifuged at 12000 g at 4°C for 15 minutes. Aqueous layer was transferred to a new microcentrifuge tube. After that, Isopropanol (500 μl) was added to each sample and centrifuged at

12000 g at 4°C for 15 minutes. Total RNA was precipitated forms a white gel-like pellet at the bottom of the tube. The supernate was removed and mixed with 500 µl of 75% ethanol. Samples were centrifuged at 7500 g at 4°C for 5 minutes and removed the supernate. The sample was air dry the RNA pellet for 5-10 minutes. Finally, the RNA pellet was resuspended in 20 µl of DepC. RNA concentration was determined using a NanoDrop spectrophotometer.

To generate complementary DNA (cDNA), at least of RNA 2 µg was used as template in a reverse transcriptase reaction. The quantitative PCR (qPCR) method was modified from Ashley et al., 2015. Primers for real time PCR were listed in Table 3.1. For each reaction primer mix tubes and cDNA mix tubes were prepared. Primer tubes contained 5 µl 2X SYBR Select master mix, 2 µl of 2 µM primer mix, and 3 µl deionized water per reaction. cDNA mixtures contained 5 µl of 2X SYBR Select master mix, 2 µl of cDNA, and 3 µl of deionized water per reaction. 10 µl each of primer mix and cDNA mix were added to the wells of a MicroAmp Fast Optical 96-well reaction plate. Plates were sealed with optical adhesive film (Life Technologies, 4311971) and run in an ABI 7500 real time PCR system using the following program: (1) 50°C for 2 min, (2) 95°C for 2 min, (3) 95°C for 15 sec, (4) 60°C for 1 min, (5) repeat 3–4 40X. Single products were confirmed by determining melting curves at the conclusion of the reaction. Relative expression was calculated using the $2^{-\Delta\Delta C_t}$ method normalized to β -actin.

Table 3.1 Realtime PCR primer name and sequence.

Gene	Sequence (5' to 3')	Size (bp)
<i>β-actin</i>	Forward: AGAGCTACGAGCTGCCTGAC Reverse: AGCACTGTGTTGGCGTACAG	189
<i>HES1</i>	Forward: CCAAGCTGGAGAAGGCGGACATTC Reverse: ACGTGGACAGGAAGCGGGTCAC	165
<i>HEY1</i>	Forward: GGATCACCTGAAAATGCTGCATAC Reverse: CCGAAATCCCAAACCTCCGATAG	126
<i>MYC</i>	Forward: AATGAAAAGGCCCCCAAGGTAGTTATCC Reverse: GTCGTTTCCGCAACAAGTCCTCTTC	112

Ref: (Park et al., 2013)

3.3.9 Statistical analysis

All data were presented as means \pm standard deviation (S.D) of three independent experiments. Differences among groups were analyzed by one way analysis of variance (ANOVA) followed by Bonferroni test for multiple comparisons. The level of statistical significant was set as p values < 0.05 . All data analyzed by SPSS program version 22.0 (Network license purchased by Chulalongkorn University).

CHAPTER IV

RESULTS AND DISCUSSION

Part I Preparation of SAHM1-PEG-gold nanoparticle conjugate (SAHM1-PEG-AuNP)

4.1 Optimization of SAHM1 peptide for conjugation on gold nanoparticle

Because a suitable amount of the gold nanoparticle adsorbed on to the SAHM1 peptide can prevent the coagulation of the conjugate; the concentration of the SAHM1 peptide must be optimized. To do so, the SAHM1 at different concentrations were mixed with the gold nanoparticle. After the addition of NaCl to the mixture, the absorbance value at 520 nm (λ_{max} of AuNP) was measured. To obtain stabilized SAHM1-AuNP conjugate, the concentration of SAHM1 must be optimized to prevent aggregation of the AuNP. Absorbance and UV-Visible spectrum of the mixture solutions prepared at different concentrations of SAHM1 was shown in Figure 4.1. High absorbance value was obtained when the SAHM1 concentration was not suitable and the aggregation of the AuNP occurred. The result showed that the minimal concentrations of SAHM1 to stabilize the AuNP were in the range of the 16.25 ± 1.25 , 31.3 ± 0.8 and 62.5 ± 1.93 μM .

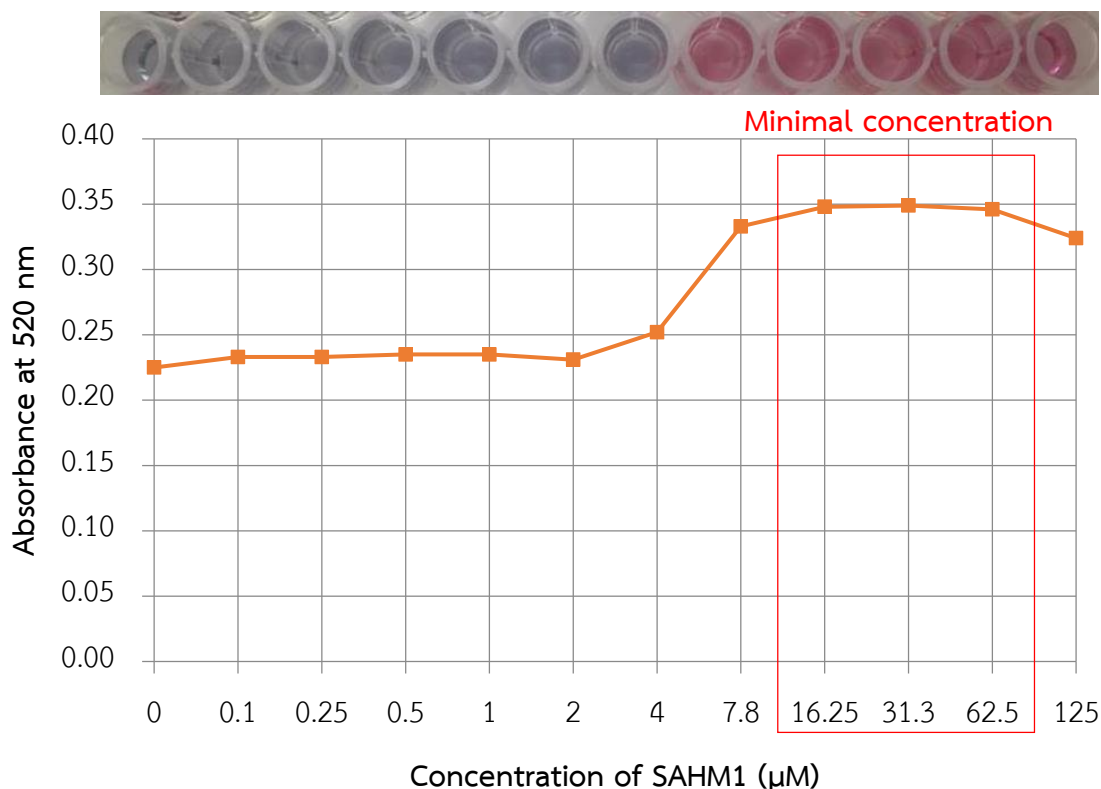


Figure 4.1 The absorbance values of SAHM1-PEG-AuNP conjugation. Solution color and the relation curve of SAHM1 concentration with respect to the absorbance at 520 nm. The result showed the minimal concentration of SAHM1 to stabilize the gold nanoparticle.

4.2 Preparation and characterization of SAHM1-PEG-gold nanoparticle conjugate (SAHM1-PEG-AuNP)

AuNP exhibited high electromagnetic waves absorption in the visible range. The spectral position of the localized surface plasmon resonance (LSPR) depends on the particle size. Generally, AuNP sized between 2 and 40 nm exhibits a LSPR band at around 520 nm (Larguinho & Baptista, 2012). Moreover, when SAHM1 is attached on the surfaces of the AuNP, they shifted the position of the LSPR to a long wavelength or red shift (Seydack, 2005).

SAHM1-PEG-AuNP was confirmed by scanning visible absorbance at 400 to 800 nm. The visible wavelength spectrum of AuNP and SAHM1-PEG-AuNP conjugate were

presented in Figure 4.2. A peak of AuNP (40 nm) was detected at 523 nm while that of SAHM1-PEG-AuNP conjugate at concentration 16.25, 31.30 and 62.5 μM were displayed at 523, 527 and 527 nm, respectively, indicating the shift of the maximum absorption wavelength.

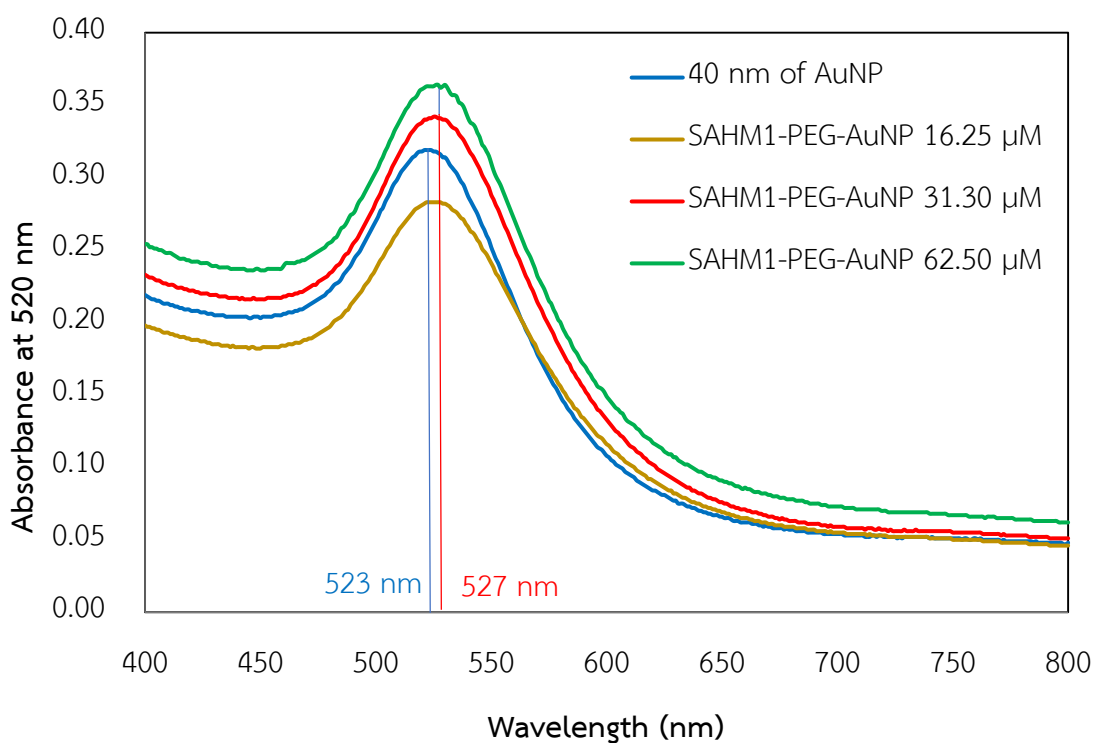


Figure 4.2 UV-Visible spectrum of AuNP in size 40 nm and SAHM1-PEG-AuNP conjugate. Concentration of SAHM1-PEG-AuNP was 16.25, 31.30 and 62.50 μM of triplicate determination.

TEM images of the AuNP, AuNP-PEG and SAHM1-PEG-AuNP conjugate were shown in Figure 4.3, 4.4 and 4.5, respectively. The results showed that most particles took spherical shape even after conjugation to SAHM1. The size of SAHM1-PEG-AuNP was larger than that of the AuNP and AuNP-PEG. The size distribution of the particles from TEM images were measured by count of a least 100 the particles by Image J analysis program. The results showed that the highest count frequency of SAHM1-PEG-AuNP conjugate particle size ranged from 45-50 nm while AuNP and AuNP-PEG were

showed particle size ranged from 30-45 and 35-40 nm. This result confirmed that the conjugation of SAHM1 and PEG to AuNP was successful.

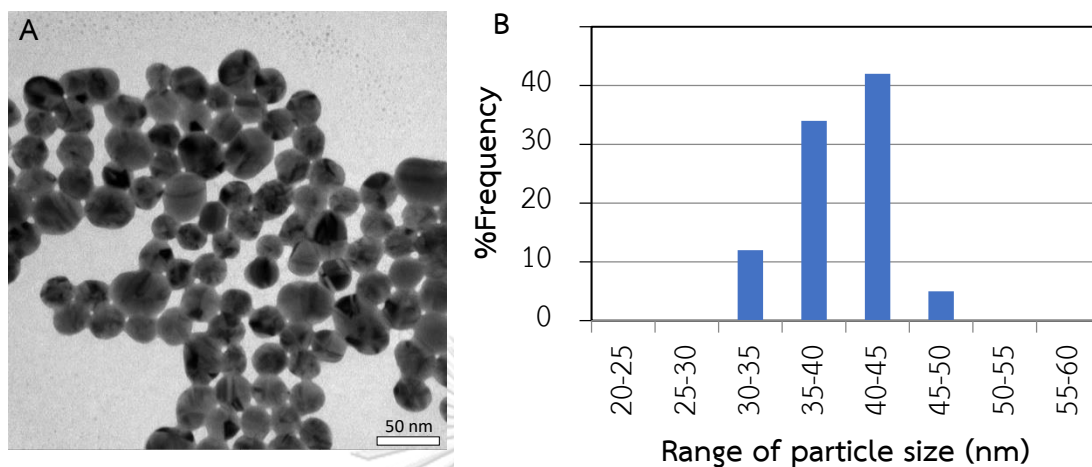


Figure 4.3 TEM image (A) and frequency of particle size distribution graph (B) of AuNP (size 40 nm). Scale bar is equivalent to 50 nm.

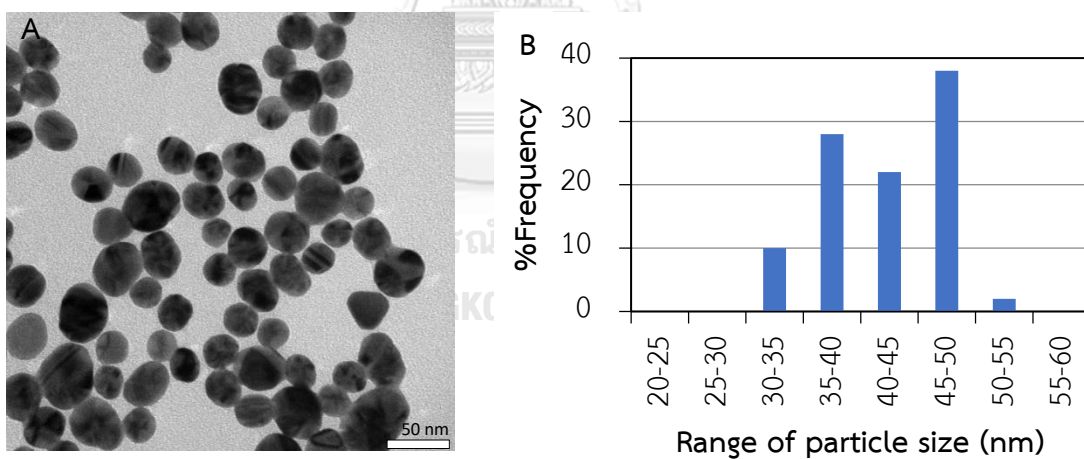


Figure 4.4 TEM image (A) and frequency of particle size distribution (B) of AuNP-PEG. Scale bar is equivalent to 50 nm.

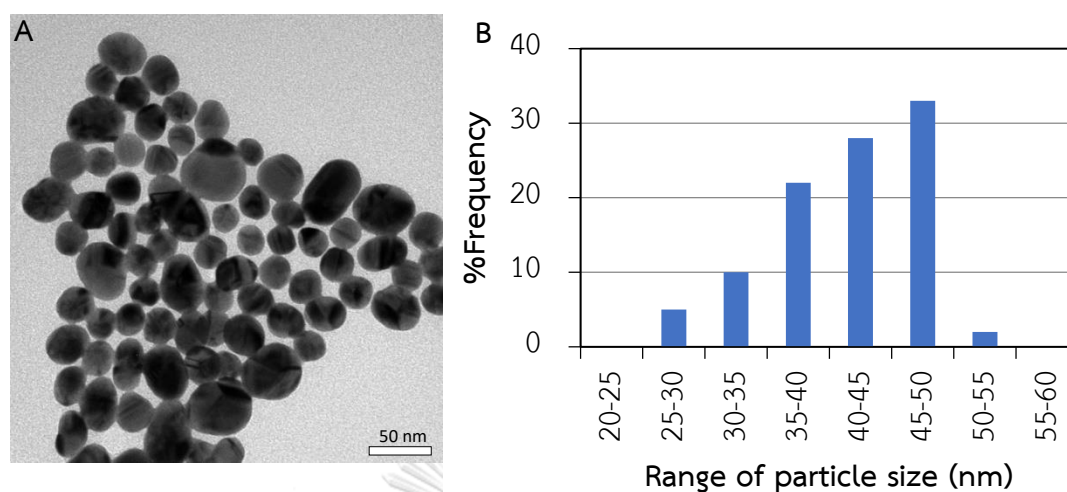


Figure 4.5 TEM image (A) and frequency of particle size distribution graph (B) of SAHM1-PEG-AuNP. Scale bar is equivalent to 50 nm.

Part II Cytotoxicity test

4.3 Cytotoxicity of the unconjugate SAHM1

The level of toxicity was calculated in term of the 50% inhibition concentration (IC_{50}) which is the least concentration of the SAHM1 that causes the 50% reduction of cell viability at any given time. The cytotoxicity of unconjugate SAHM1 alone was evaluated by MTT assay. For Jurkat cell line, the MTT assay showed that the SAHM1 was toxic to the cells. The IC_{50} of SAHM1 against Jurkat cell line after treatment for 24, 48 and 72 h were 82.73 ± 3.46 , 65.67 ± 2.31 and 17.54 ± 5.17 μ M, respectively as shown in Figure 4.6.

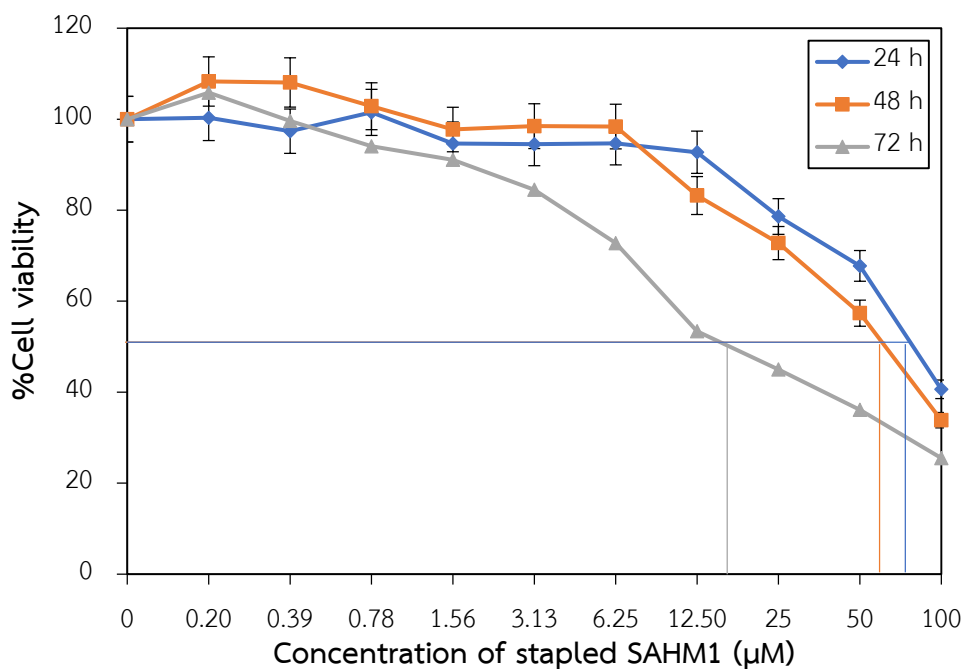


Figure 4.6 Cytotoxicity of Jurkat cell line after treatment with SAHM1 (0-100 μM) for 24, 48 and 72 h. Error bars represent mean \pm SD of triplicate determination.

Effect of SAHM1 on the morphology of Jurkat cell line was investigated. Cells were treated with different concentrations of SAHM1 for 24, 48 and 72 h and the morphology was observed under an inverted microscope as shown in Figure 4.7. It could be seen that the untreated cells (A, C and E) showed round shape morphology. On the contrary, cells treated with SAHM1 (B, D and F) showed dark cell morphology. Numbers of cells were also decreased significantly upon SAHM1 treatment. These indicated that SAHM1 alone was toxic to Jurkat cell lines.

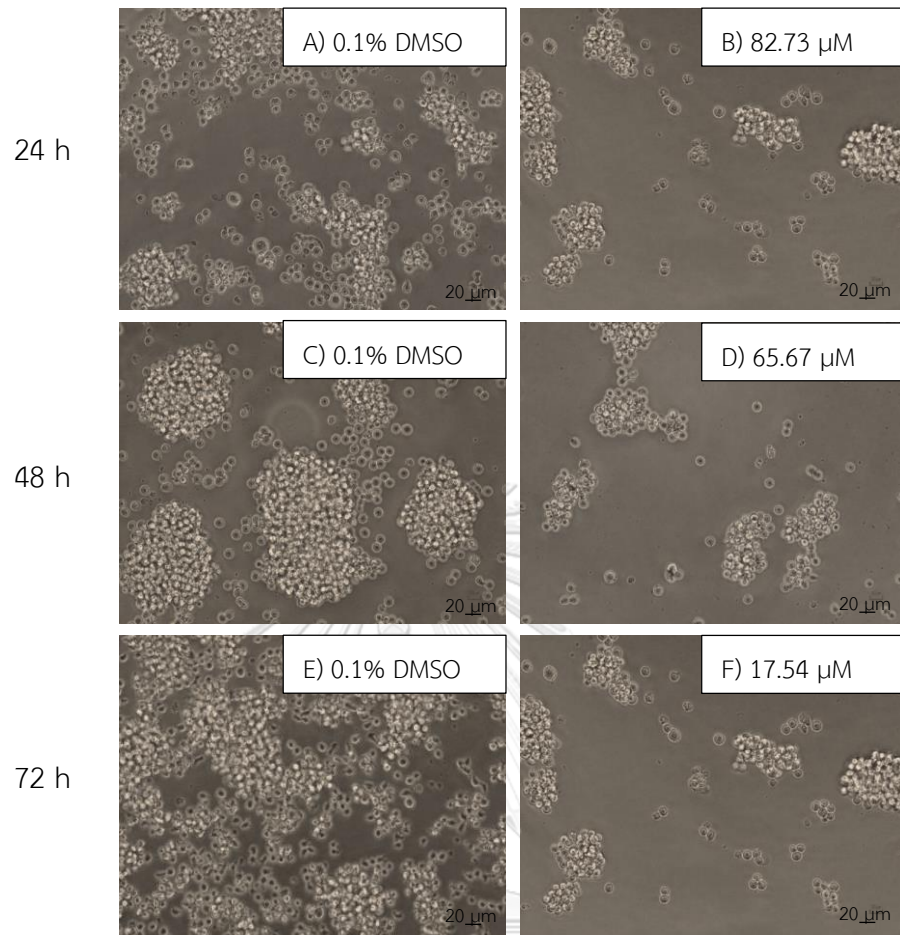


Figure 4.7 Morphology of Jurkat cell line after treatment with SAHM1. The image A, C and E were control (0.1% DMSO) and B, D and F were treated with 82.73, 65.67 and 17.54 μM of SAHM1 for 24, 48 and 72 h. All images were taken at the magnification of 200X and the scale bar was 20 μm .

4.4 Cytotoxicity of DAPT

Notch signaling pathway can be effectively inhibited with γ -secretase inhibitors, such as N-[N-(3, 5-difluorophenacetyl-L-alanyl)]-(S)-phenylglycine t-butyl ester (DAPT). In this study, DAPT was used as the positive control to inhibit Notch signaling pathway. DAPT was attached Notch complex for MAML1 was not attached Notch complex. Therefore, DAPT inhibited Notch signaling pathway.

The cytotoxicity of DAPT was detected by MTT assay in Jurkat cell line. The MTT assay showed that the DAPT was highly toxic to the cells. The IC_{50} of DAPT against Jurkat cell line after treatment for 48 and 72 h was 54.56 ± 3.47 and 20.22 ± 4.15 μM , respectively as shown in Figure 4.8.

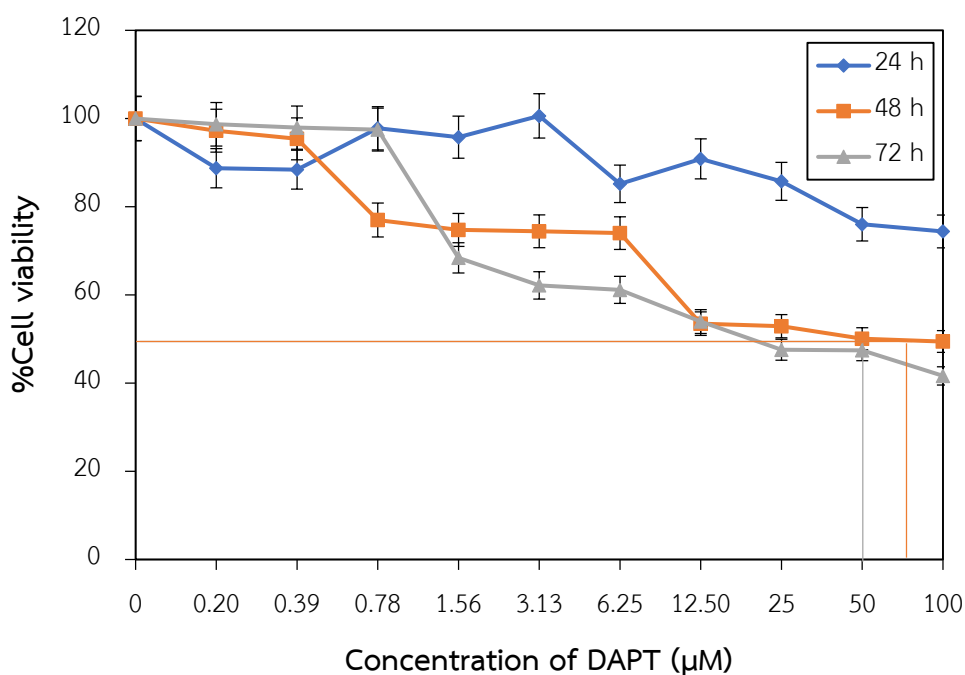


Figure 4.8 Cytotoxicity of Jurkat cell line after treatment with DAPT. Concentrations of DAPT (0-100 μM) for 24, 48 and 72 h. Error bars represent mean \pm SD of triplicate determination.

Effect of DAPT on the morphology of Jurkat cell line was studied. Cells were treated with different concentrations of DAPT for 24, 48 and 72 h and the morphology was observed under an inverted microscope as shown in Figure 4.9. It could be seen that the untreated cells (A, C and E) showed round shape morphology. On the contrary, cells treated with DAPT (B, D and F) showed dark cell morphology. Numbers of cells were also decreased significantly upon DAPT treatment. These indicated that DAPT alone was toxic to Jurkat cell lines.

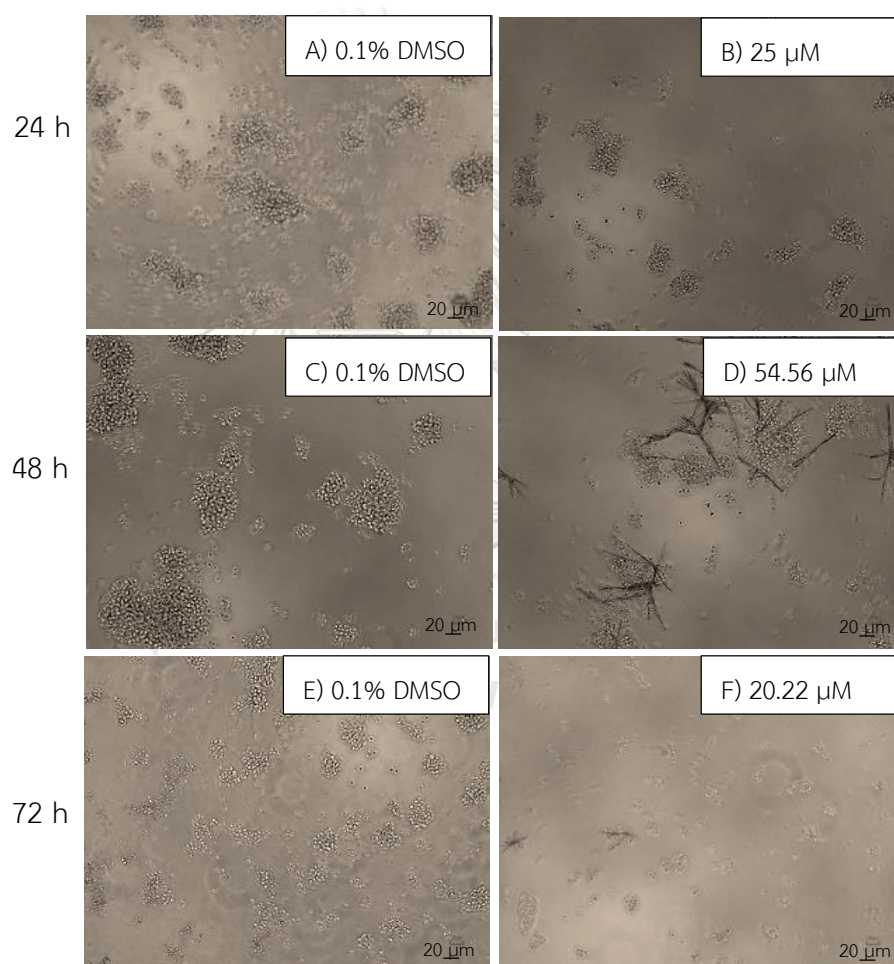


Figure 4.9 Microscopic examination of Jurkat cell line after treatment for 24, 48 and 72 h. The image A, C and E were control (0.1% DMSO) and B, D and F were treated with 25, 54.56 and 20.22 μM of SAHM1. All images were taken at the magnification of 200X and the scale bar was 20 μm .

4.5 Cytotoxicity of gold nanoparticle

Cytotoxicity of gold nanoparticle (AuNP) was detected by MTT assay (Figure 4.10). Different concentrations of AuNP (size 40 nm) were treated in Jurkat cell line for 24, 48 and 72 h. These result showed that AuNP at all tested concentrations were nontoxic to the cells. Effect of AuNP on the morphology of Jurkat cell line after treatment with AuNP was observed under an inverted microscope as shown in Figure 4.11. Cells were treated with different concentrations of AuNP for 24, 48 and 72 h. The result showed that the control (A, C, and E) have round shape morphology. The result showed that after treatment (B, D and F) was round shape similar to those of the untreated cell. Therefore, AuNP can be used as drug carrier in Jurkat cell line without obvious toxicity.

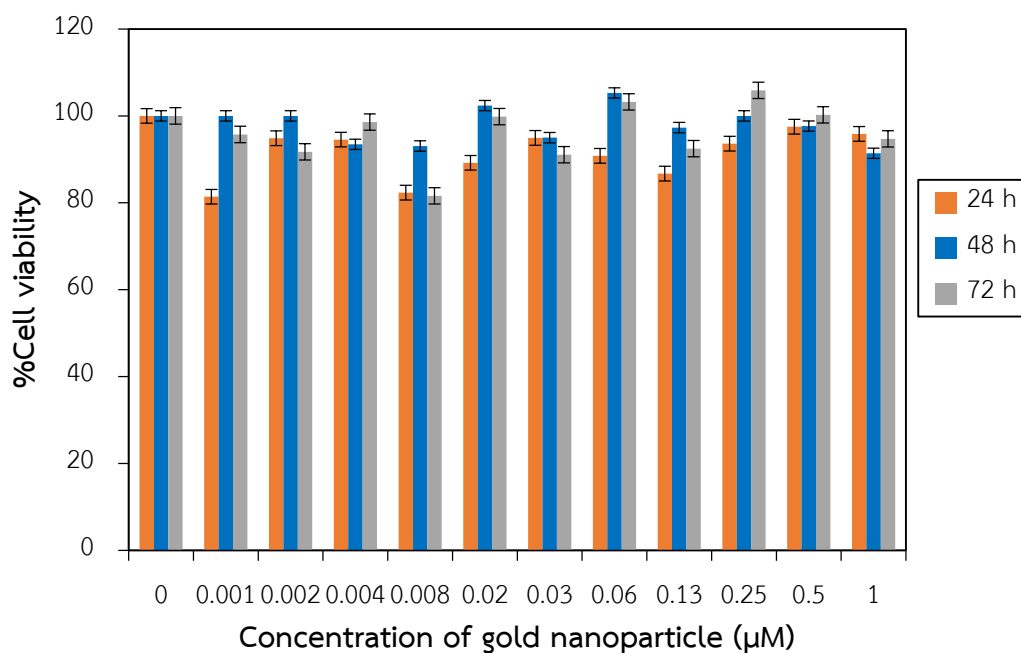


Figure 4.10 Cytotoxicity of AuNP in Jurkat cell line evaluated by MTT assay. %Cell viability after treatment of AuNP (0.001-1 µM) for 24, 48 and 72 h. Error bars represent mean \pm SD of triplicate determination.

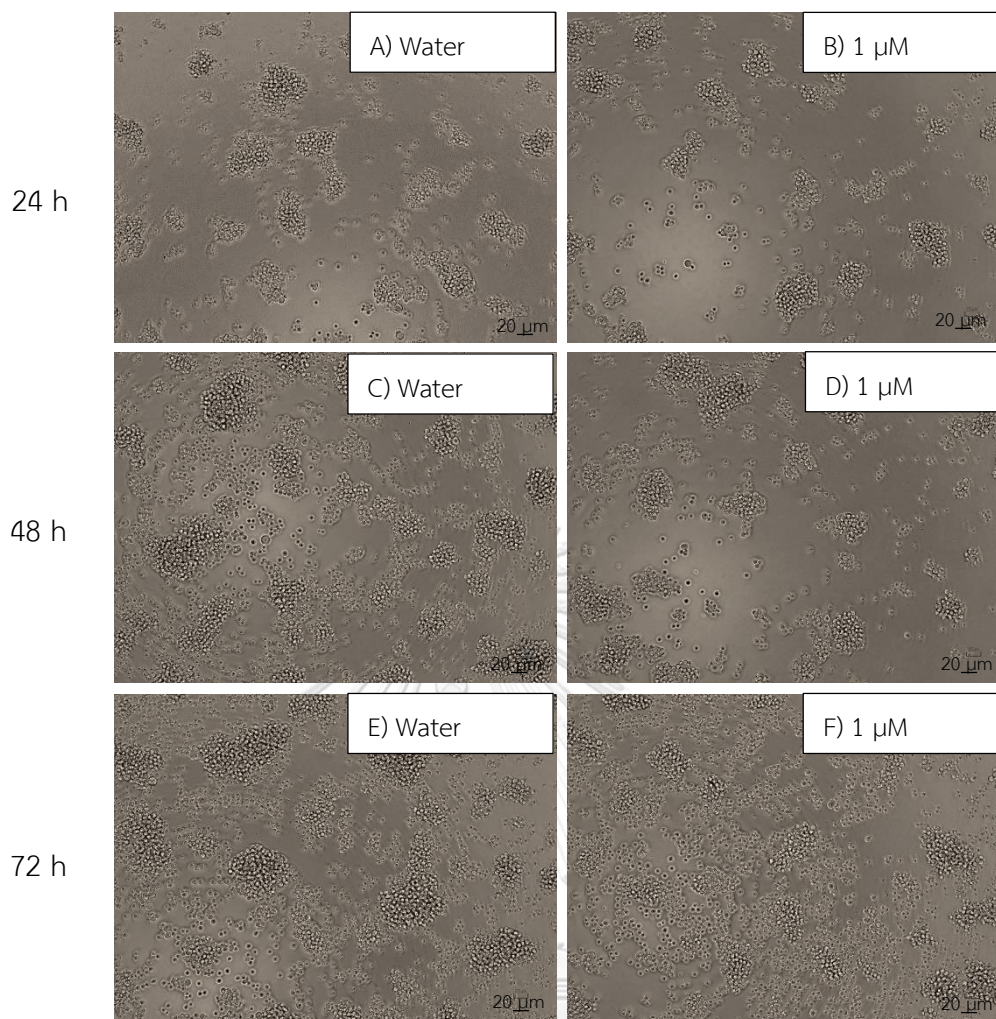


Figure 4.11 Morphology and distribution of Jurkat cell line after treatment. The image A, C and E were control (sterile water) and B, D and F were treated with 40 nm of AuNP for 24, 48 and 72 h. All images were taken at the magnification of 200X and the scale bar was 20 μm.

4.6 Cytotoxicity of PEG

The cytotoxicity of PEG on Jurkat cell line after treatment with different concentrations of PEG for 24, 48 and 72 h was tested by MTT assay and the result was shown in Figure 4.12. These result showed that all concentrations of PEG was not toxic to the cells. Effect of PEG on the morphology of Jurkat cell line was studied. Cells were treated with different concentrations of PEG for 24, 48 and 72 and the morphology was observed under an inverted microscope as shown in Figure 4.13. Furthermore, the result showed that the control (A, C, and E) have round-like morphology cell and normal cell. The result showed that after treatment (B, D and F) was round shape similar to untreated. Therefore, PEG was used for conjugation of SAHM1 with AuNP.

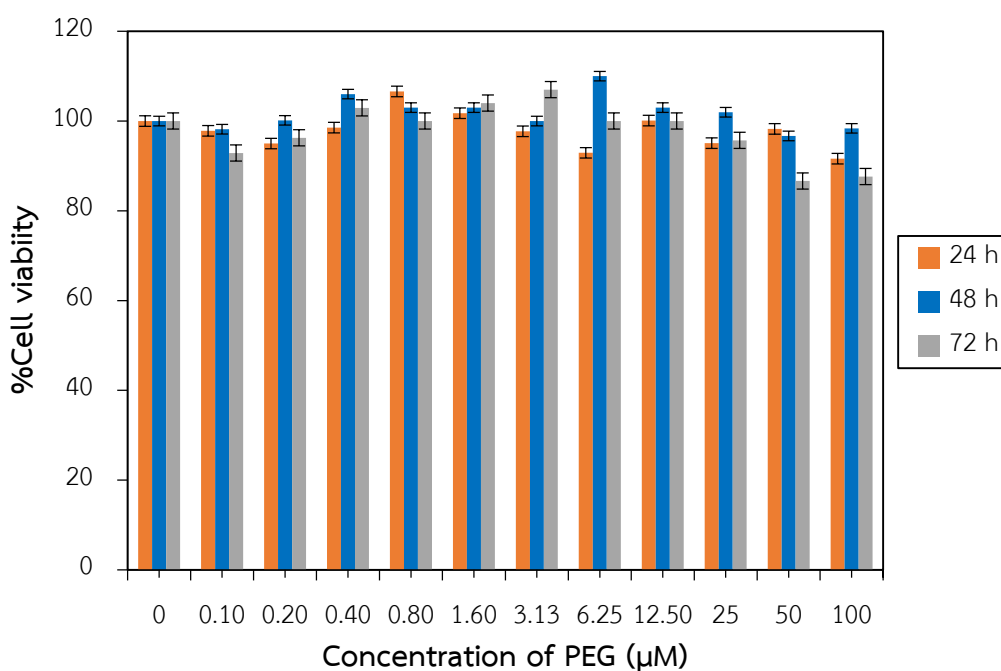
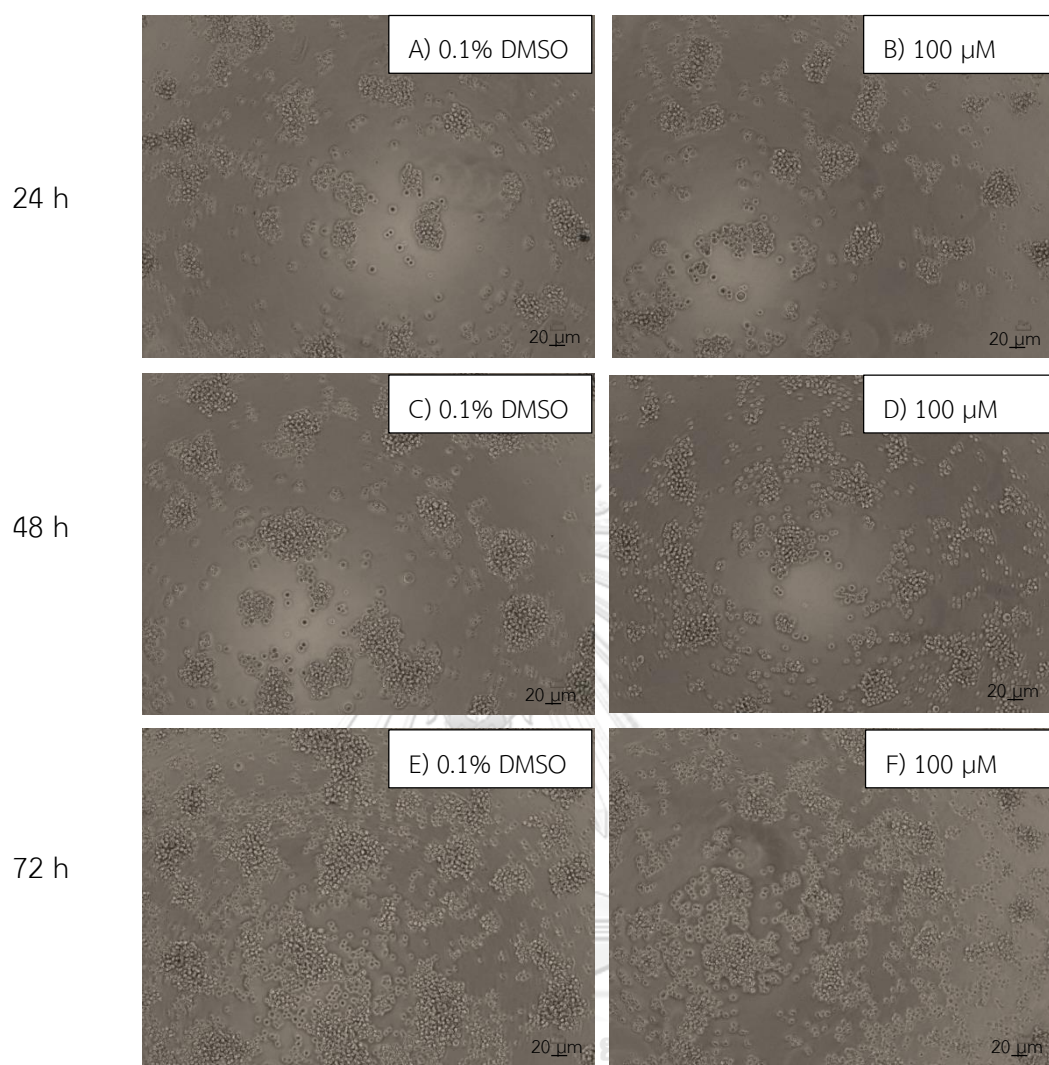


Figure 4.12 Cytotoxicity of PEG in Jurkat cell line evaluated by MTT assay. %Cell viability after treatment with PEG (0-100 μM) for 24, 48 and 72 h. Error bars represent mean \pm SD of triplicate determination.



CHULALONGKORN UNIVERSITY

Figure 4.13 Microscopic examination of Jurkat cell line after treatment. The image A, C and E were control (0.1% DMSO) and B, D and F were treated with 100 μM of PEG for 24, 48 and 72 h. All images were taken at the magnification of 200X and the scale bar was 20 μm.

4.7 Cytotoxicity of SAHM1-PEG-AuNP

In previous study, Park et al., 2013 used cell penetrating peptide and conjugated with AuNP (size 40 and 60 nm) in 3 types of cancer cell (Hela, A549 and 3T3-L1). The result reported that cell penetrating peptide was increased cytotoxicity when compare with unconjugated. AuNP (size 40 nm) was increased cell penetrating activity than AuNP (size 60 nm).

In this work, stapled SAHM1 (cell penetrating peptide) was conjugated with AuNP (size 40 nm) and studied cytotoxicity by MTT assay. Percent cell viability of Jurkat cells treated with DAPT (50 μ M), SAHM1, AuNP, PEG, AuNP-PEG and SAHM1-PEG-AuNP conjugate at different concentrations (16.25, 31.3 and 62.5 μ M) showed in Figure 4.14, 4.15 and 4.16, respectively. It could be seen that AuNP alone was not toxic while unconjugated SAHM1 was high toxic to the cell. Importantly, % cell viability of the cells treated with SAHM1-PEG-AuNP was lower than that of the cells treated with unconjugated SAHM1, thus indicating the increase significantly in SAHM1 toxicity due to the conjugation. In addition, cell death induced by SAHM1-PEG-AuNP was increased. SAHM1-PEG-AuNP showed enhanced cytotoxicity compared with unconjugated SAHM1 and AuNP-PEG without SAHM1. However, more studies are required to elucidate this enhancement. It might be due to either the increase in the stability of SAHM1 inside the cells or the increase in the amount of SAHM1 which penetrates into the cells.

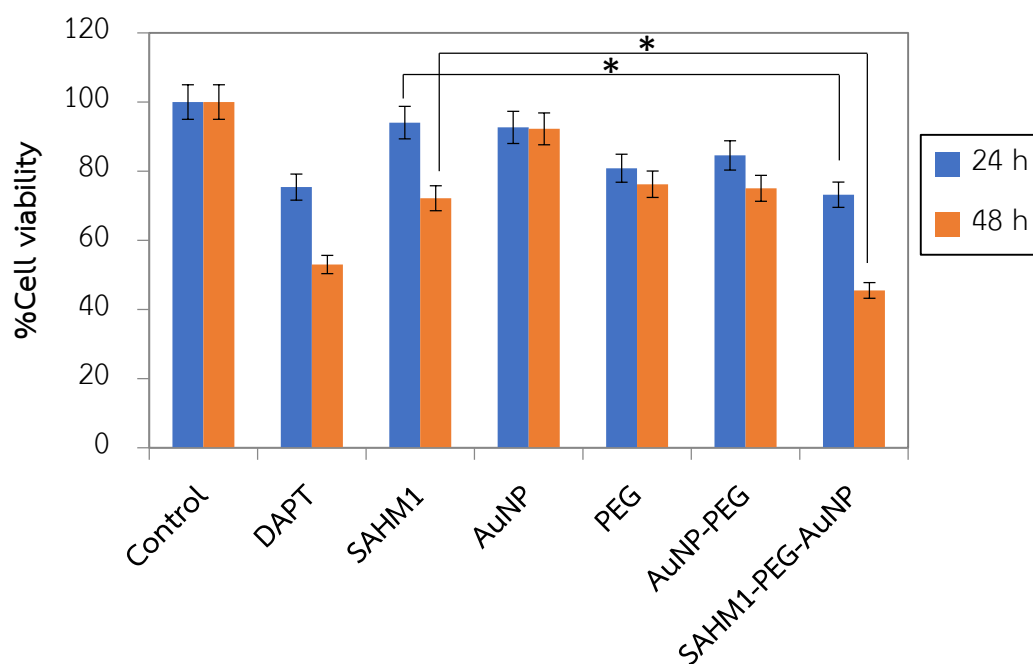


Figure 4.14 %Cell viability of Jurkat cell line after treatment with different reagents. Cytotoxicity of DAPT (50 μM), SAHM1 (16.25 μM), AuNP (16.25 μM), PEG (16.25 μM), AuNP-PEG (16.25 μM) and SAHM1-PEG-AuNP conjugate for 24 and 48 h, error bars represent mean \pm SD of triplicate determination, * $p < 0.05$.

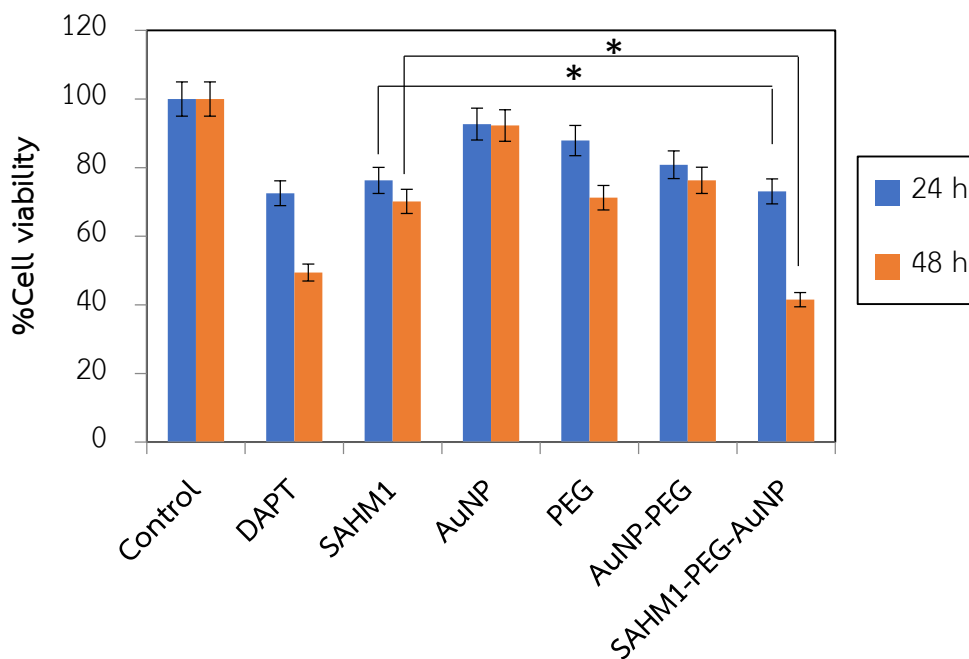


Figure 4.15 %Cell viability of Jurkat cell line after treatment with different reagents. Cytotoxicity of DAPT (50 μ M), SAHM1 (31.3 μ M), AuNP (31.3 μ M), PEG (31.3 μ M), AuNP-PEG (31.3 μ M) and SAHM1-PEG-AuNP conjugate for 24 and 48 h, error bars represent mean \pm SD of triplicate determination, * $p < 0.05$.

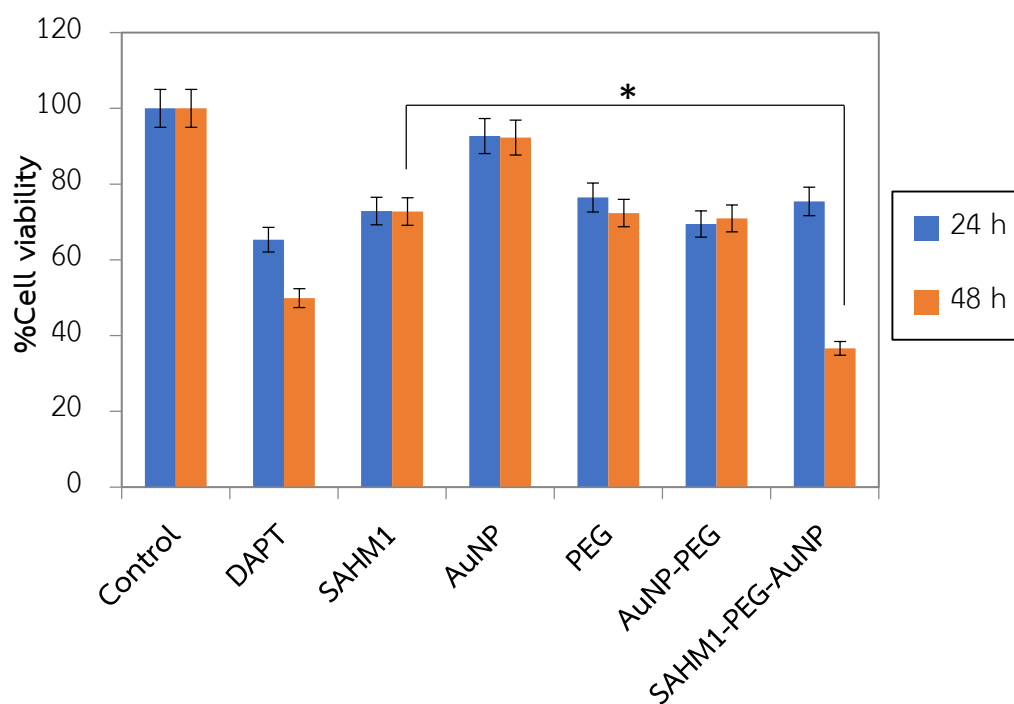
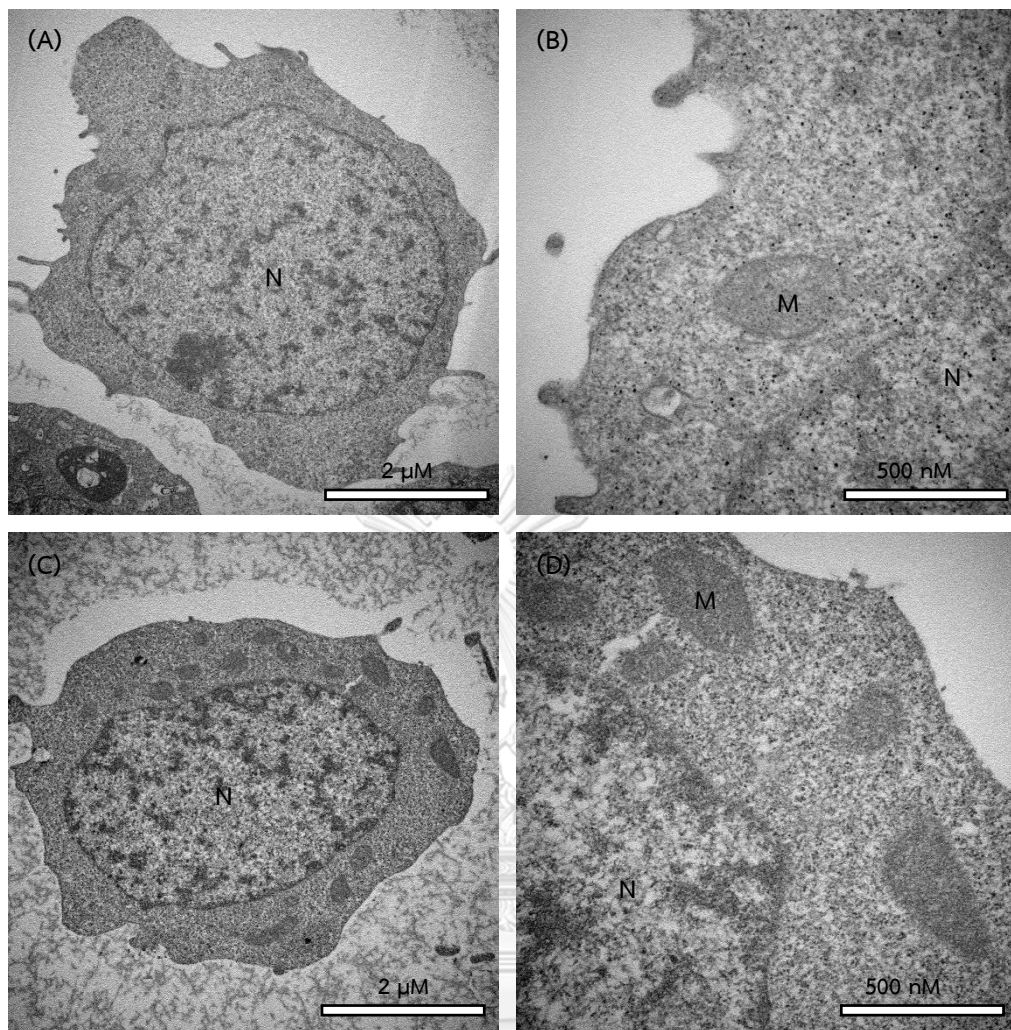


Figure 4.16 %Cell viability of Jurkat cell line after treatment with different reagents. Cytotoxicity of DAPT (50 μ M), SAHM1 (62.5 μ M), AuNP (62.5 μ M), PEG (62.5 μ M), AuNP-PEG (62.5 μ M) and SAHM1-PEG-AuNP (62.5 μ M) for 24 and 48 h, error bars represent mean \pm SD of triplicate determination, * $p < 0.05$.

Part III Internalization and localization of SAHM1-PEG-AuNP

Internalization and localization of SAHM1-PEG-AuNP were detected by TEM cell section analysis. TEM images of section for Jurkat cell line after incubation without AuNP (Control) for 24 h was showed in Figure 4.17 (A and B). The result showed that normal cell was large nucleus and oval in shape. Figure 4.17 showed the TEM images of section for Jurkat cell line after incubation with SAHM1 (31.3 μM) for 24 h. Figure 4.18 showed the TEM images of section from Jurkat cell line after incubation AuNP (31.3 μM) for 24 h. Wang et al., 2010, Liu et al., 2013 and Laksee et al., 2017 reported that AuNP was trapped in the endosome in HepG2 and KATO-III cells. To test this hypothesis, the cellular uptake of SAHM1-PEG-AuNP was evaluated using TEM. Jurkat cell lines cultured without SAHM1-PEG-AuNP contained large nucleus. Figure 4.20 showed TEM images of section after incubation SAHM1-PEG-AuNP (31.3 μM) for 24 h. Cells exposure to SAHM1-PEG-AuNP had accumulated AuNP of SAHM1-PEG-AuNP conjugate in cytoplasm the Jurkat cell line (Figure 4.20), presumably following endocytosis of the AuNP (Wang et al., 2010). In addition, AuNP-PEG without SAHM1 was not founded in the Jurkat cell line (Figure 4.19) similar to the unconjugated AuNP. These results suggested that AuNP was taken into the Jurkat cell line via endocytosis and thus will likely have transported SAHM1 peptide into the cell, resulting in the enhanced cytotoxicity. From all results, internalization of SAHM1-PEG-AuNP had better than unconjugated AuNP. Hence, this investigation suggests that SAHM1-PEG-AuNP could act as carrier for anticancer drug delivery system in biomedical applications.



จุฬาลงกรณ์มหาวิทยาลัย

Figure 4.17 TEM image of section in Jurkat cell line after incubation without AuNP (A and B) and treated with 31.3 μM of SAHM1 (C and D) for 24 h. Low magnification of a whole cell section (A and C) and high magnification of part of cell section (B and D). Intracellular feature labeled as nucleus (N) and mitochondria (M).

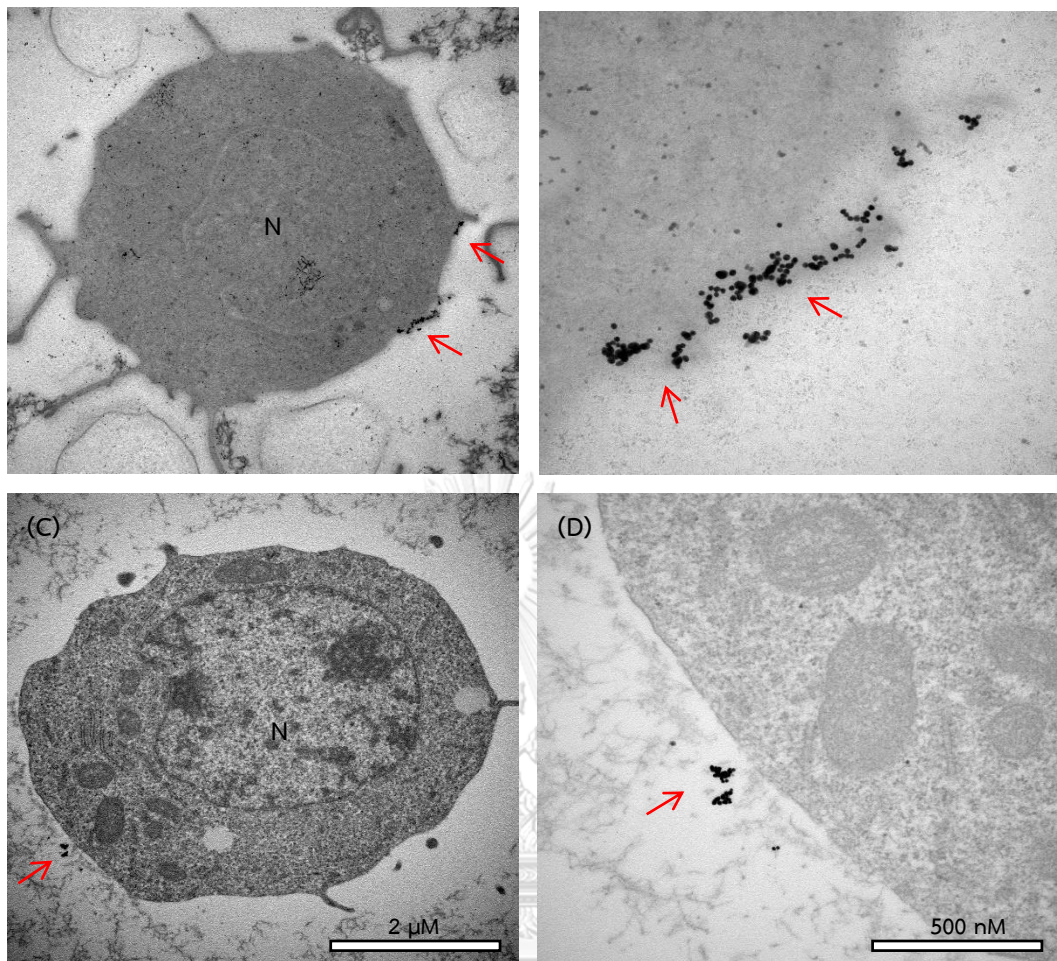


Figure 4.18 TEM image of Jurkat cell line after treatment with AuNP (31.3 μM) for 24 h. Low magnification of a whole cell section (A and C) and high magnification of part of cell section (B and D). Red arrows marked AuNP, intracellular feature labeled as nucleus (N).

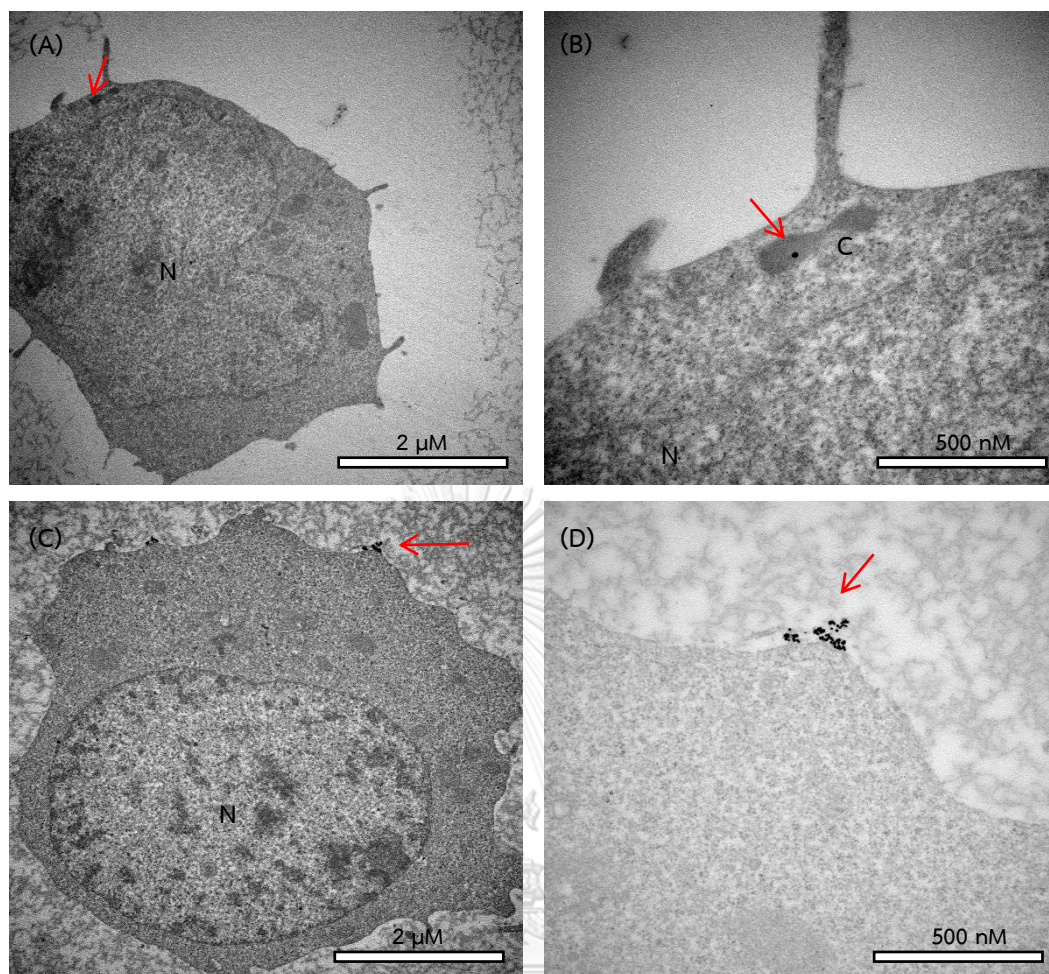


Figure 4.19 Representative TEM images of section for Jurkat cell line after treatment with AuNP-PEG (31.3 μM) for 24 h. Low magnification of a whole cell section (A and C) and high magnification of part of cell section (B and D). Red arrows marked AuNP, intracellular feature labeled as cytoplasm (C) and nucleus (N).

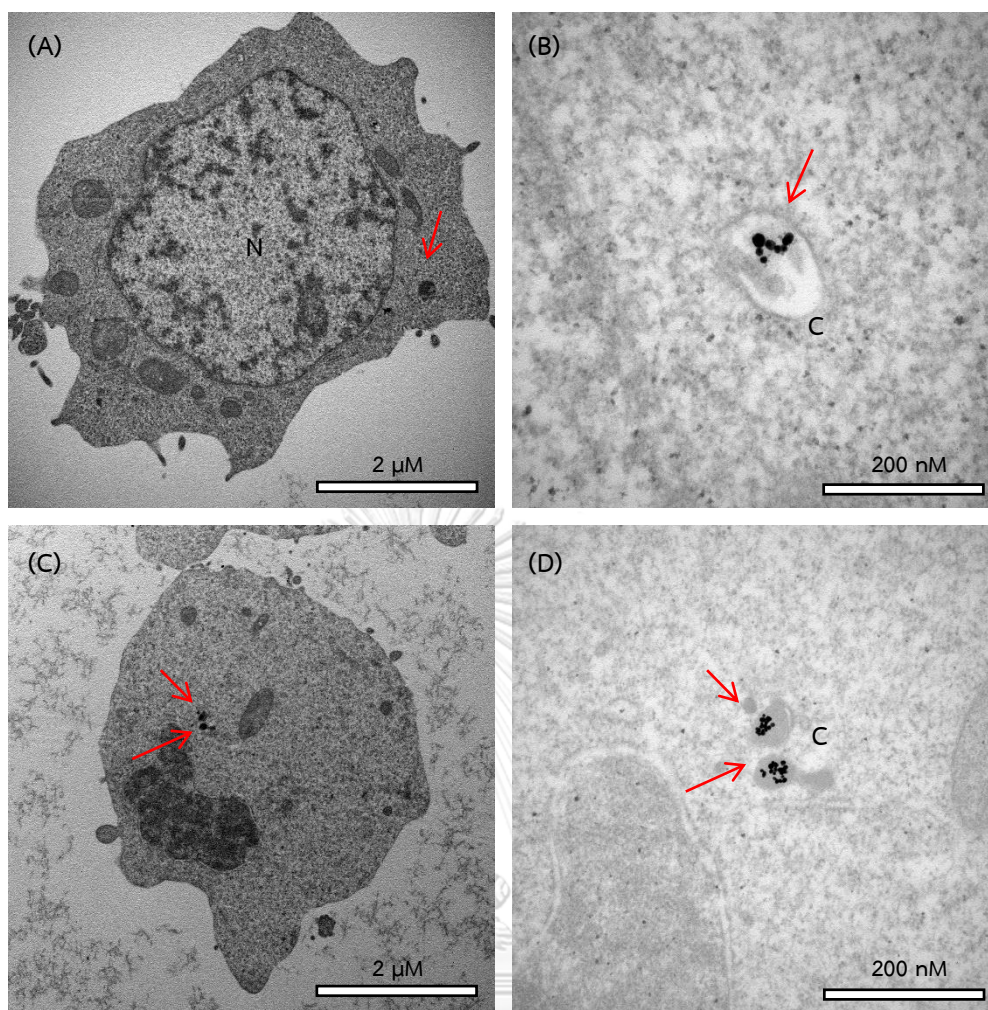


Figure 4.20 TEM images of Jurkat cell line after incubation with SAHM1-PEG-AuNP (31.3 μM) for 24 h. Low magnification of a whole cell section (A and C) and high magnification of part of cell section (B and D). Red arrows marked AuNP, intracellular feature labeled as cytoplasm (C) and nucleus (N).

Part IV Effect of SAHM1-PEG-AuNP on Notch signaling pathway

The effect of SAHM1 on the expression of Notch target genes (*HES1*, *HEY1* and *MYC*) in Jurkat cell line was measured by quantitative PCR (qPCR). Jones et al., 2009 reported that exposure of cells to SAHM1 peptide significantly reduced transcription of *HES1* and *MYC* and other Notch target genes, whereas various mutant peptides were relatively inactive. Verdine et al., 2010 reported that T-cell acute lymphoblastic leukemia (T-ALL) cells featuring deregulated Notch were treated with the SAHM1 peptide and RT-PCR was performed to demonstrate a dose-dependent inhibition of expression of Notch-dependent target genes. Figure 4.21 showed qPCR result of the Notch target genes in Jurkat cell line after treatment with DAPT (50 μM), SAHM1 (31.3 μM), AuNP (31.3 μM), PEG (31.3 μM), AuNP-PEG (31.3 μM) and SAHM1-PEG-AuNP (31.3 μM) relative to dimethylsulphoxide (DMSO) control for 48 h. The result show that AuNP (size 40 nm), PEG and AuNP-PEG without SAHM1 peptide at concentration 31.3 μM was increased the expression level of Notch target genes (*HES1*, *HEY1* and *MYC*). Consequently, the AuNP, PEG and AuNP-PEG did not affect the Notch signaling pathway in Jurkat cell line. DAPT (γ -secretase inhibitor) was positive control and the result showed that DAPT treatment decreased expression level of the Notch target genes. While SAHM1-PEG-AuNP was not significantly decreased expression level of the Notch target genes when compare with unconjugated SAHM1. Analysis of Notch target gene levels induced by SAHM1 confirmed specific repression of the Notch signaling pathway in Jurkat cell line.

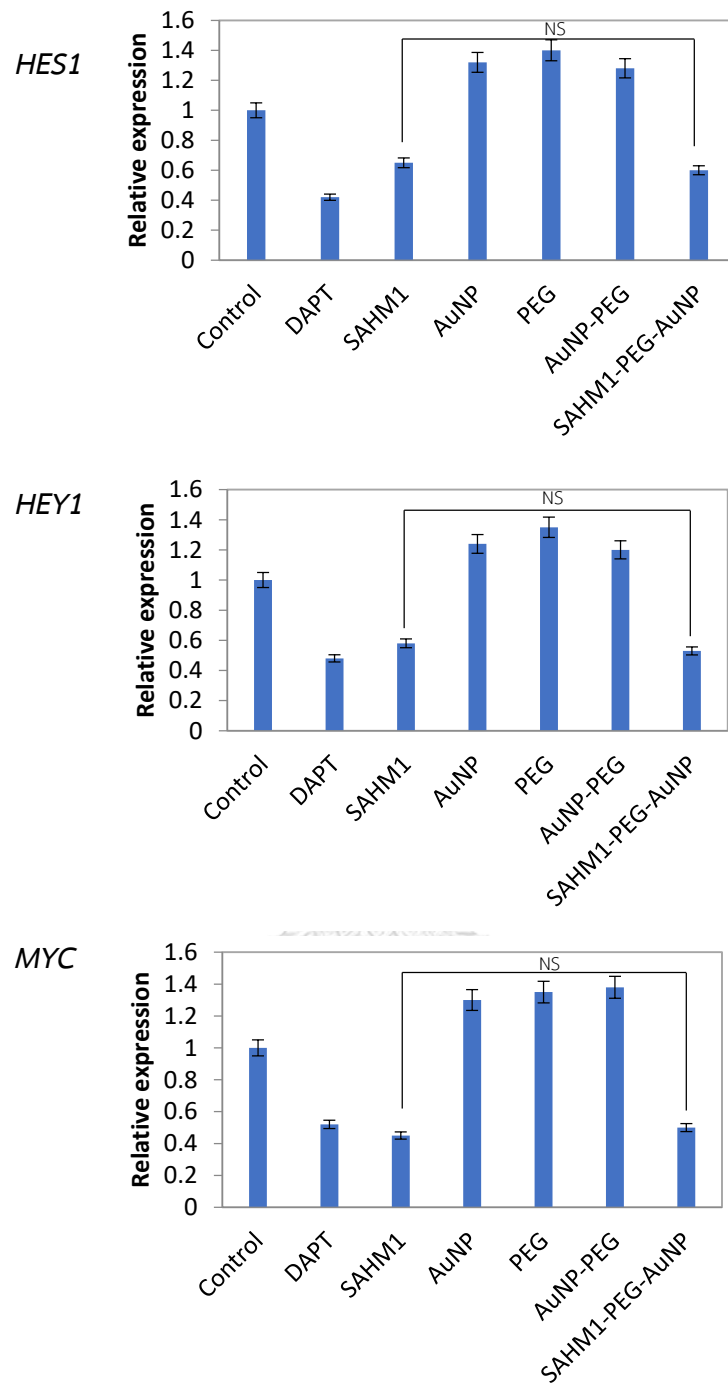


Figure 4.21 Effect of SAHM1 on the expression of Notch target genes. qPCR analysis of the *HES1*, *HEY1* and *MYC* mRNA levels in Jurkat cell line treated for 48 h with DAPT, SAHM1, AuNP, PEG, AuNP-PEG and SAHM1-PEG-AuNP relative to dimethylsulphoxide (DMSO) control. Error bars represent mean \pm SD of triplicate determination, not statistical significant (NS).

CHAPTER V

CONCLUSION

In summary, development of target delivery system by using AuNP (carrier) was conjugated with PEG (linker) and SAHM1 peptide (anticancer peptide). It was found that to successfully conjugation. The optimum concentration of PEG and SAHM1 were 31.3 μM , while that of AuNP was 100 μM . The size of the SAHM1-PEG-AuNP was estimated to be 45-50 nm. The UV-visible spectrum showed the shift peak at the wavelength 527 nm. The cytotoxicity test was determined by MTT assay and the cell morphology was observed under the inverted fluorescence microscope in Jurkat cell line. The result demonstrated that SAHM1-PEG-AuNP was increased significantly toxicity while unconjugated AuNP and PEG were not toxic. The internalization and localization of SAHM1-PEG-AuNP were detected by TEM section analysis. The result showed that SAHM1-PEG-AuNP was trapped in cytoplasm but unconjugated AuNP was not founded in Jurkat cell line. The effect of SAHM1-PEG-AuNP on Notch signaling pathway was measured by qPCR of Notch target genes (*HES1*, *HEY1* and *MYC*). The result showed that the expression level of Notch target gene was not significantly decreased when compared with unconjugated SAHM1. Therefore, SAHM1-PEG-AuNP was increased toxicity by inhibition of Notch signaling pathway in Jurkat cell line. These all results summarized that SAHM1-PEG-AuNP would be a useful tool for the development of new drug delivery system.

REFERENCES

- Adam, G. (2003). The retinoic-like juvenile hormone controls the looping of left-right asymmetric organs in *Drosophila*. *Development*, *130*(11), 2397-2406.
- Aribi, A., Borthakur, G., Ravandi, F., Shan, J., Davissou, J., Cortes, J., & Kantarjian, H. (2007). Activity of decitabine, a hypomethylating agent, in chronic myelomonocytic leukemia. *Cancer*, *109*(4), 713-717.
- Arnaiz, B., Martinez-Avila, O., Falcon-Perez, J. M., & Penades, S. (2012). Cellular uptake of gold nanoparticles bearing HIV gp120 oligomannosides. *Bioconjugate Chemistry*, *23*(4), 814-825.
- Ashley, J. W., Ahn, J., & Hankenson, K. D. (2015). Notch signaling promotes osteoclast maturation and resorptive activity. *Journal of Cellular Biochemistry*, *116*(11), 2598-2609.
- Aster, J. C., Pear, W. S., & Blacklow, S. C. (2008). Notch signaling in leukemia. *Annual Review of Pathology*, *3*, 587-613.
- Athar, M., & Das, J. A. (2013). Therapeutic nanoparticles: State-of-the-art of nanomedicine. *Advanced Materials Reviews*, *1*(1), 25-37.
- Boisselier, E., & Astruc, D. (2009). Gold nanoparticles in nanomedicine: preparations, imaging, diagnostics, therapies and toxicity. *Chemical Society Reviews*, *38*(6), 1759-1782.
- Brandelli, A. (2012). Nanostructures as promising tools for delivery of antimicrobial peptides. *Mini-Reviews in Medicinal Chemistry*, *12*(8), 731-741.
- Cabuzu, D., Cirja, A., Puiu, R., & Grumezescu, A. M. (2015). Biomedical applications of gold nanoparticles. *Current Topics in Medicinal Chemistry*, *15*(16), 1605-1613.
- Cao-Milan, R., & Liz-Marzan, L. M. (2014). Gold nanoparticle conjugates: recent advances toward clinical applications. *Expert Opinion Drug Delivery*, *11*(5), 741-752.
- Chiodo, F., Marradi, M., Calvo, J., Yuste, E., & Penades, S. (2014). Glycosystems in nanotechnology: Gold glyconanoparticles as carrier for anti-HIV prodrugs. *Beilstein Journal of Organic Chemistry*, *10*, 1339-1346.

- Daniel, M. C., & Astruc, D. (2004). Gold nanoparticles: assembly, supramolecular chemistry, quantum-size-related properties, and applications toward biology catalysis, and nanotechnology. *Chemical Reviews*, *104*(1), 293-346.
- Dykman, L. A., & Khlebtsov, N. G. (2011). Gold nanoparticles in biology and medicine: recent advances and prospects. *Acta Naturae*, *3*(2), 34-55.
- Ferlay, J., Shin, H. R., Bray, F., Forman, D., Mathers, C., & Parkin, D. M. (2010). Estimates of worldwide burden of cancer in 2008. *The International Journal of Cancer*, *127*(12), 2893-2917.
- Frens, G. (1973). Controlled nucleation for the regulation of the particle size in monodisperse gold suspensions. *Nature*, *241*, 20-22.
- Hafez, H. A., Solaiman, R., Bilal, D., & Shalaby, L. (2016). Early Deaths in Pediatric Acute Leukemia; A Challenge in Developing Countries. *Blood*, *128*(22), 5160-5165.
- Hainfeld, J. F., Dilmanian, F. A., Zhong, Z., Slatkin, D. N., Kalef-Ezra, J. A., & Smilowitz, H. M. (2010). Gold nanoparticles enhance the radiation therapy of a murine squamous cell carcinoma. *Physics and Medicine Biology*, *55*(11), 3045-3059.
- He, H., Xie, C., & Ren, J. (2008). Nonbleaching fluorescence of gold nanoparticles and its applications in cancer cell imaging. *Analytical Chemistry*, *80*(15), 5951-5957.
- Horikoshi, S., & Serpone, N. (2013). *Microwaves in Nanoparticle Synthesis*.
- Huo, S., Ma, H., Huang, K., Liu, J., Wei, T., Zhang, J., . . . Liang, X. J. (2013). Superior penetration and retention behavior of 50 nm gold nanoparticles in tumors. *Cancer Research*, *73*(1), 319-330.
- Jain, S., Hirst, D. G., & O'Sullivan, J. M. (2012). Gold nanoparticles as novel agents for cancer therapy. *The British of Journal Radiology*, *85*(1010), 101-113.
- Jakobs, R. T. M., van Herrikhuyzen, J., Gielen, J. C., Christianen, P. C. M., Meskers, S. C. J., & Schenning, A. P. H. J. (2008). Self-assembly of amphiphilic gold nanoparticles decorated with a mixed shell of oligo(p-phenylene vinylene) s and ethyleneoxide ligands. *Journal of Materials Chemistry*, *18*(29), 3438-3441.
- Jazayeri, M. H., Amani, H., Pourfatollah, A. A., Pazoki-Toroudi, H., & Sedighimoghaddam, B. (2016). Various methods of gold nanoparticles (GNPs) conjugation to antibodies. *Sensing and Bio-Sensing Research*, *9*, 17-22.

- Jones, K. A. (2009). Outsmarting a mastermind. *Developmental Cell*, 17(6), 750-752.
- Kim, E. Y., Kumar, D., Khanga, G., & Lim, D. K. (2015). Recent advances in gold nanoparticle-based bioengineering applications. *Journal of Materials Chemistry B*, 3(43), 8433-8444.
- Kimling, J., Maier, M., Okenve, B., Kotaidis, V., Ballot, H., & Plech, A. (2006). Turkevich method for gold nanoparticle synthesis revisited. *The Journal of Physical Chemistry B*, 110(32), 15700-15707.
- Larguinho, M., & Baptista, P. V. (2012). Gold and Silver Nanoparticles for Clinical Diagnostics-From Genomics to Proteomics. *Journal of Proteomics*, 75(10), 2811-2823.
- Ljungblad, J. (2009). Antibody-conjugated gold nanoparticles integrated in a fluorescence based biochip.
- Moellering, R. E., Cornejo, M., Davis, T. N., Del Bianco, C., Aster, J. C., Blacklow, S. C., . . . Bradner, J. E. (2009). Direct inhibition of the NOTCH transcription factor complex. *Nature*, 462(7270), 182-188.
- Park, H., Tsutsumi, H., & Mihara, H. (2013). Cell penetration and cell-selective drug delivery using alpha-helix peptides conjugated with gold nanoparticles. *Biomaterials*, 34(20), 4872-4879.
- Parkin, D. M. (2006). The global health burden of infection-associated cancers in the year 2002. *International journal of cancer*, 118(12), 3030-3044.
- Patra, C. R., Bhattacharya, R., Mukhopadhyay, D., & Mukherjee, P. (2010). Fabrication of gold nanoparticles for targeted therapy in pancreatic cancer. *Advanced Drug Delivery Reviews*, 62(3), 346-361.
- Schneider, U., Schwenk, H., & Bornkamm, G. (1977). Characterization of EBV-genome negative "null" and "T" cell lines derived from children with acute lymphoblastic leukemia and leukemic transformed non-Hodgkin lymphoma. *International journal of cancer*, 19(5), 621-626.
- Seydack, M. (2005). Nanoparticle labels in immunosensing using optical detection methods. *Biosensors and Bioelectronics*, 20(12), 2454-2469.

- Verdine, G. L., & Hilinski, G. J. (2012). Stapled peptides for intracellular drug targets. *Methods in Enzymology*, 503, 3-33.
- Wang, H., Xu, K., Liu, L., Tan, J. P., Chen, Y., Li, Y., . . . Li, L. (2010). The efficacy of self-assembled cationic antimicrobial peptide nanoparticles against *Cryptococcus neoformans* for the treatment of meningitis. *Biomaterials*, 31(10), 2874-2881.
- Wang, H., Zheng, L., Guo, R., Peng, C., Shen, M., Shi, X., & Zhang, G. (2012). Dendrimer-entrapped gold nanoparticles as potential CT contrast agents for blood pool imaging. *Nanoscale Research Letters*, 7, 190.
- Zhang, X. (2015). Gold Nanoparticles: Recent Advances in the Biomedical Applications. *Cell Biochemistry and Biophysics*, 72(3), 771-775.
- Zhao, C., Zhong, G., Kim, D. E., Liu, J., & Liu, X. (2014). A portable lab-on-a-chip system for gold-nanoparticle-based colorimetric detection of metal ions in water. *Biomicrofluidics*, 8(5), 052107.
- Zhou, Y., Andersson, O., Lindberg, P., & Liedberg, B. (2004). Reversible Hydrophobic Barriers Introduced by Microcontact Printing: Application to Protein Microarrays. *Microchimica Acta*, 146(3), 193-205.



APPENDICES

จุฬาลงกรณ์มหาวิทยาลัย
CHULALONGKORN UNIVERSITY

APPENDIX A

Reagents and Buffers

1. Reagents for optimization and conjugation

1.1 10 mM SAHM1

SAHM1	1 mg
DMSO	1 ml

The solution was stored at -20°C until use.

1.2 0.2 M sodium carbonate

Sodium carbonate	2.12 g
DDI water	100 ml

2. Media for cell culture

2.1 Media for Jurkat cell line culture

RPMI 1640 (Roswell Park Memorial Institute)	10.43 g
NaHCO ₃	2 g
L-glutamine	0.1 g
Glucose	2 g
Sodium pyruvate	0.11 g
Distilled water	1000 ml

The medium was sterilized by filter membrane 0.22 µm and stored at 4°C until use.

2.2 Freezing medium (10% v/v DMSO)

Dimethyl sulfoxide (DMSO)	10 ml
PPMI-1640 medium	90 ml

The medium was stored at 4°C until use.

3. Reagents and Buffers for cell section analysis

3.1 2.5% glutaraldehyde

Glutaraldehyde	2.5 mg
0.1 M phosphate buffer	100 ml

3.2 0.01 M phosphate buffer saline, pH 7

0.2 M phosphate buffer	1000 ml
NaCl	175.2 g
DI water adjusted volume to	20 L

4. Reagent for MTT assay

4.1 5mg/ml MTT solution

MTT	5 mg
Normal saline	1 ml

The solution was stored at 4°C until use.

5. Reagent for RNA extraction

5.1 Diethylpyrocarbonate (DEPC)


0.1 % Diethylpyrocarbonate (DEPC)	1 ml
Distilled water	1000 ml

5.2 75% Ethanol

Ethanol	75 ml
DEPC	25 ml

APPENDIX B

Gold nanoparticle




**KESTREL
BIO SCIENCES**

CERTIFICATE OF ANALYSIS

KBS Thailand™
COA-CG1705001

Colloidal Gold, 40 nanometers

Product Name	Colloidal Gold, 40nm
Catalog	KP-05120003
Lot Number	030417-018-6
Volume	500 ML
Peak wave length	522.5
Absorbance	1.168
Storage	2°C - 8°C
Expiration Date	1 year from the date of receipt (May 2018)



Rinyabhat Patchararajudom (Tah) , GM

Kestrel Bio Sciences (Thailand) Co., Ltd., Certifies on the date above that this is an accurate record of the analysis of the subject lot and that the data conform to the specifications in effect for this product at the time of analysis.

Kestrel Bio Sciences (Thailand) Co., Ltd.
60/77 Moo 19, Navanakorn Ind., Zone 2
Paholyothin Rd., Klong 1, Klong Luang, Pathumthani, 12120
Mobile: +66 88 661 9156
Email: tah.kbsthailand@gmail.com

Figure B-1 Certificate of analysis of colloidal gold nanoparticle (size 40 nm)

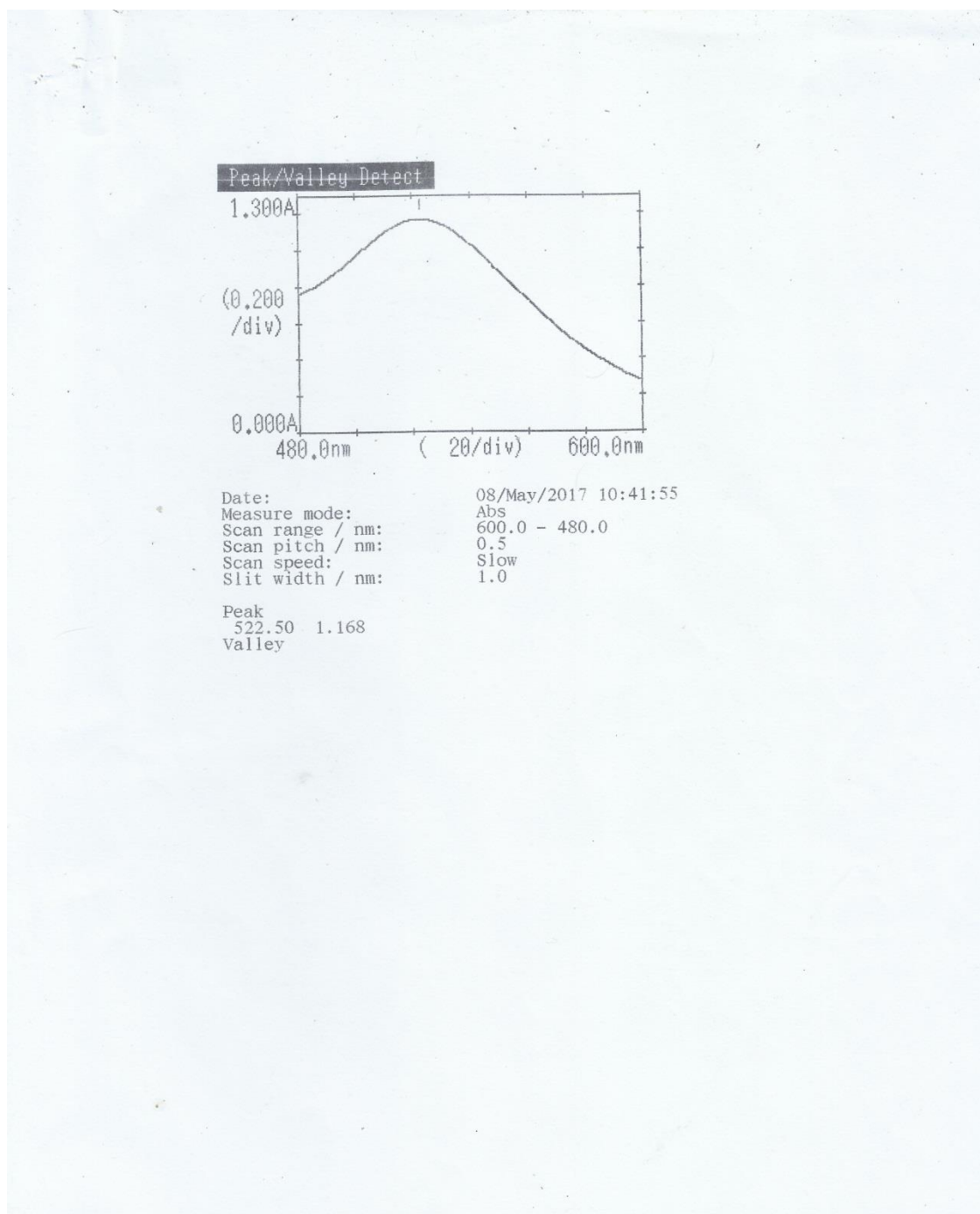
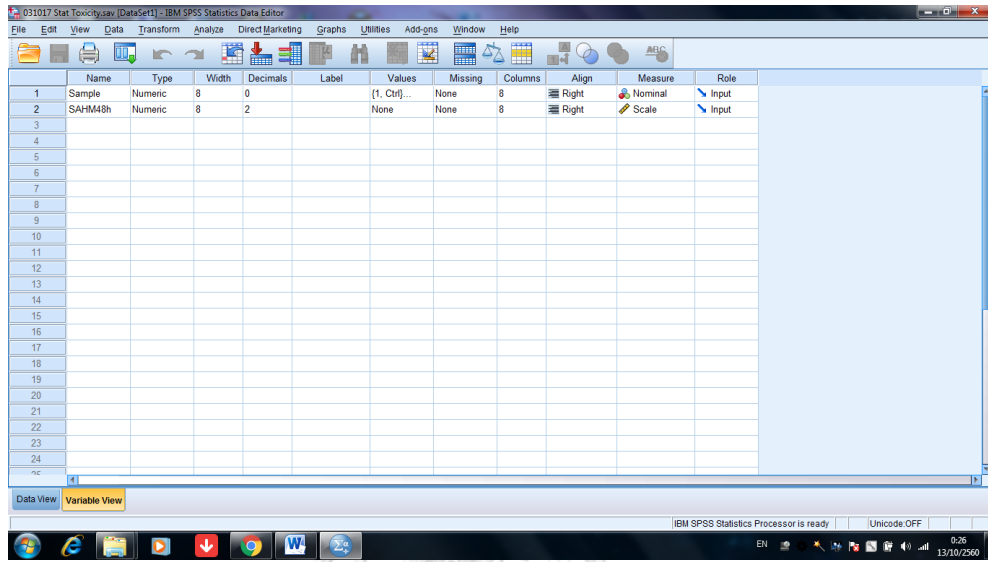


Figure B-2 Chromatogram of colloidal gold nanoparticle (size 40 nm)

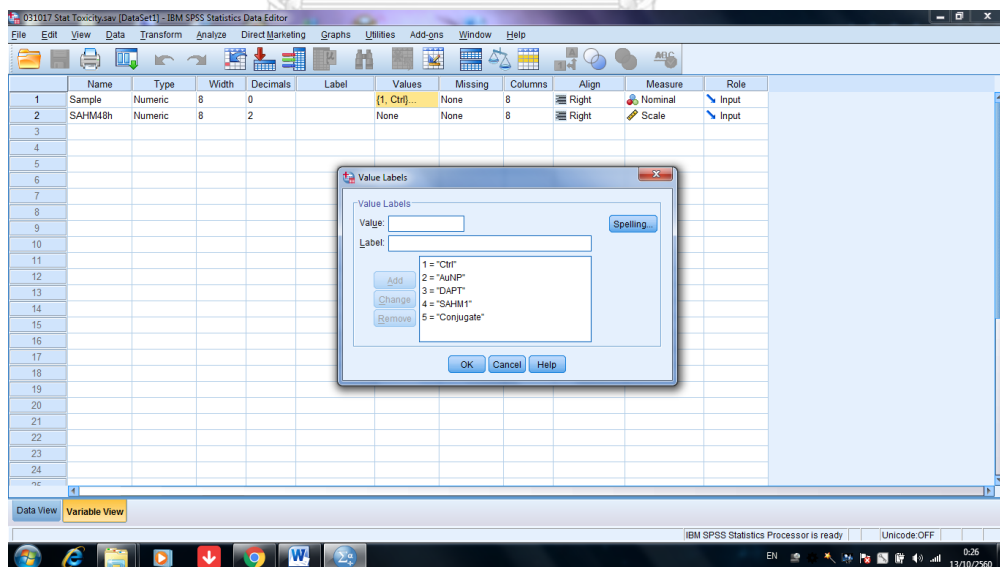
APPENDIX C

Statistics analysis

1. Open IBM SPSS Statistics 22 program



2. Select of values and key name of sample data



3. Add result of data

The screenshot shows the IBM SPSS Statistics Data Editor window. The data table is displayed in Data View. The first two columns are 'Sample' and 'SAHM48h'. The data points are as follows:

Sample	SAHM48h
1	100.00
2	100.00
3	100.00
4	98.00
5	99.00
6	97.00
7	72.00
8	82.00
9	79.00
10	88.00
11	86.00
12	91.00
13	72.00
14	76.00
15	78.00
16	
17	
18	
19	
20	
21	
22	
23	

The status bar at the bottom indicates 'IBM SPSS Statistics Processor is ready' and 'Unicode: OFF'. The system tray shows the time as 0:27 on 13/10/2560.

4. Analyze by one way anova

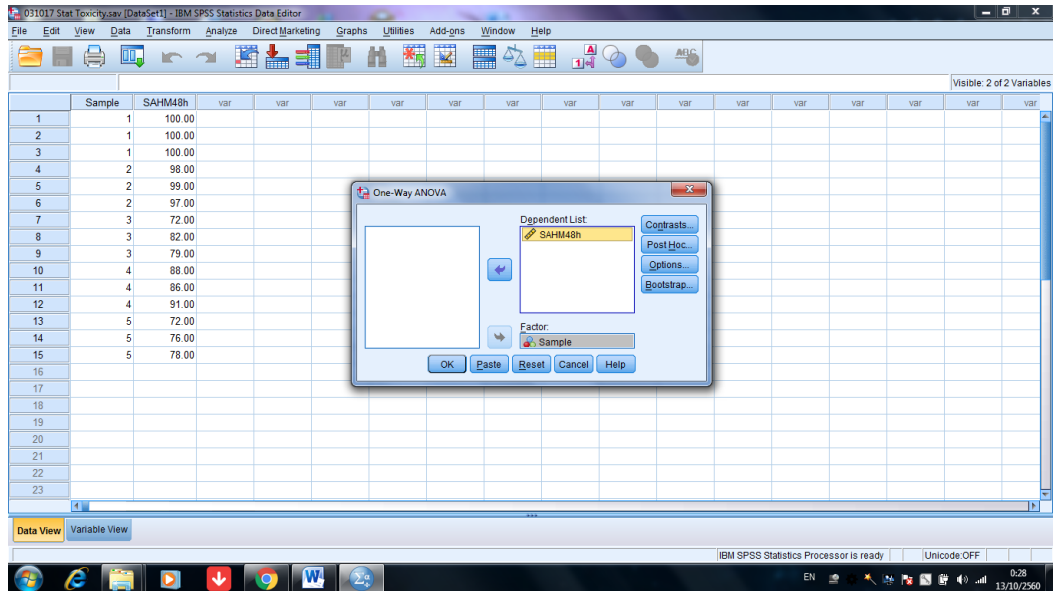
The screenshot shows the IBM SPSS Statistics Data Editor window with the 'Analyze' menu open. The 'One-Way ANOVA...' option is selected. The data table is visible in the background, showing the same data as in the previous screenshot.

The 'Analyze' menu is open, showing the following options:

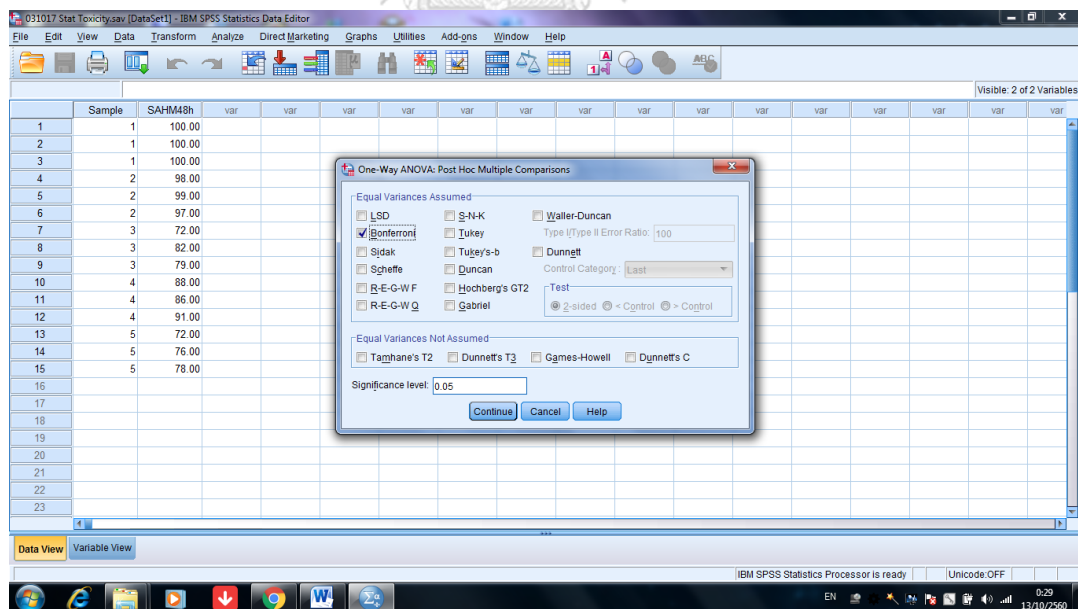
- Reports
- Descriptive Statistics
- Tables
- Compare Means
 - Means...
 - One-Sample T Test...
 - Independent-Samples T Test...
 - Paired-Samples T Test...
 - One-Way ANOVA...
- General Linear Model
- Generalized Linear Models
- Mixed Models
- Correlate
- Regression
 - Loglinear
 - Neural Networks
 - Classify
 - Dimension Reduction
 - Scale
 - Nonparametric Tests
 - Forecasting
 - Survival
 - Multiple Response
- Missing Value Analysis...
- Multiple Imputation
- Complex Samples
- Simulation...
- Quality Control
- ROC Curve...

The status bar at the bottom indicates 'IBM SPSS Statistics Processor is ready' and 'Unicode: OFF'. The system tray shows the time as 0:27 on 13/10/2560.

5. Select sample to factor and name of sample to dependent lists



6. For One-Way ANOVA, select of Bonferrini test for multiple comparison at significant 0.05



7. After finished analyze, new window of result for statistics analysis

The screenshot shows the IBM SPSS Statistics Viewer interface. The main window displays the results of a One-way ANOVA for the variable SAHM72h. The output is organized into two main sections: Descriptives and ANOVA.

Descriptives

	N	Mean	Std. Deviation	Std. Error	95% Confidence Interval for Mean		Minimum	Maximum
					Lower Bound	Upper Bound		
Ctbl	3	100.0000	.00000	.00000	100.0000	100.0000	100.00	100.00
AuNP	3	98.0000	1.00000	.57735	95.5159	100.4841	97.00	99.00
DAPT	3	69.0000	4.00000	2.30940	59.0634	78.9366	65.00	73.00
SAHM1	3	80.0000	2.00000	1.15470	75.0317	84.9683	78.00	82.00
Conjugate	3	55.3333	4.50925	2.60342	44.1317	66.5349	51.00	60.00
Total	15	80.4667	17.80797	4.59800	70.6049	90.3284	51.00	100.00

ANOVA

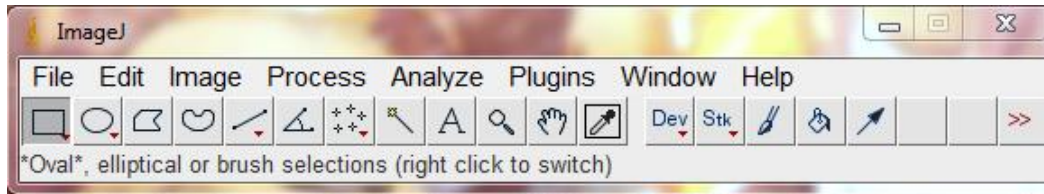
	Sum of Squares	df	Mean Square	F	Sig.
Between Groups	4357.067	4	1089.267	131.766	.000
Within Groups	82.667	10	8.267		
Total	4439.733	14			



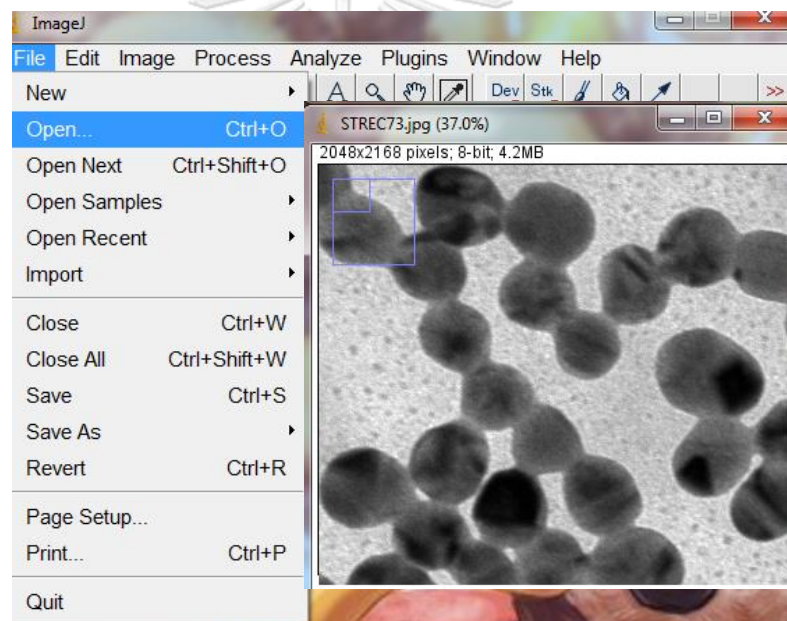
APPENDIX D

Image J analysis

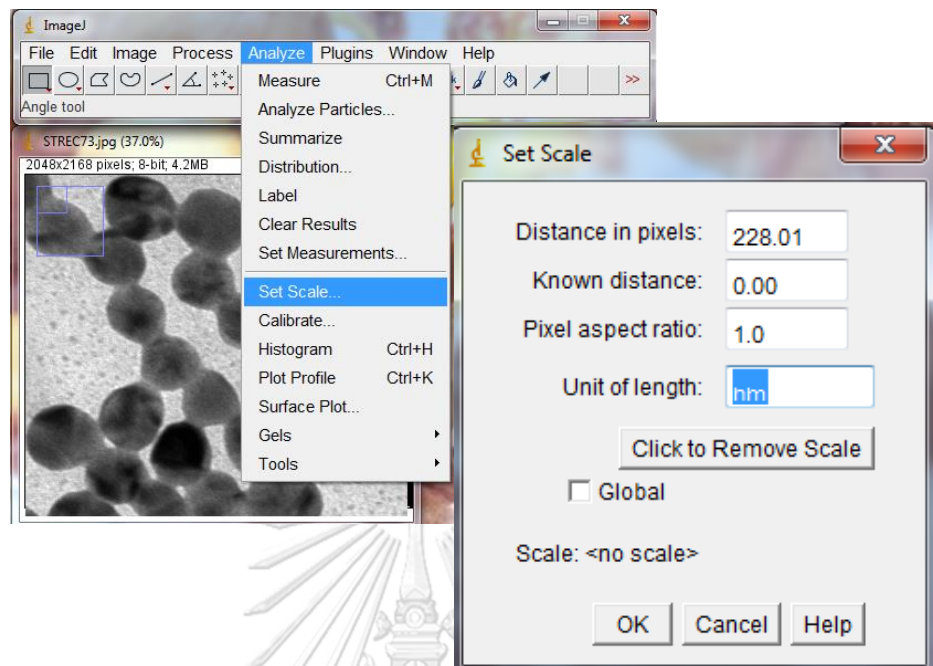
1. Open Image J program



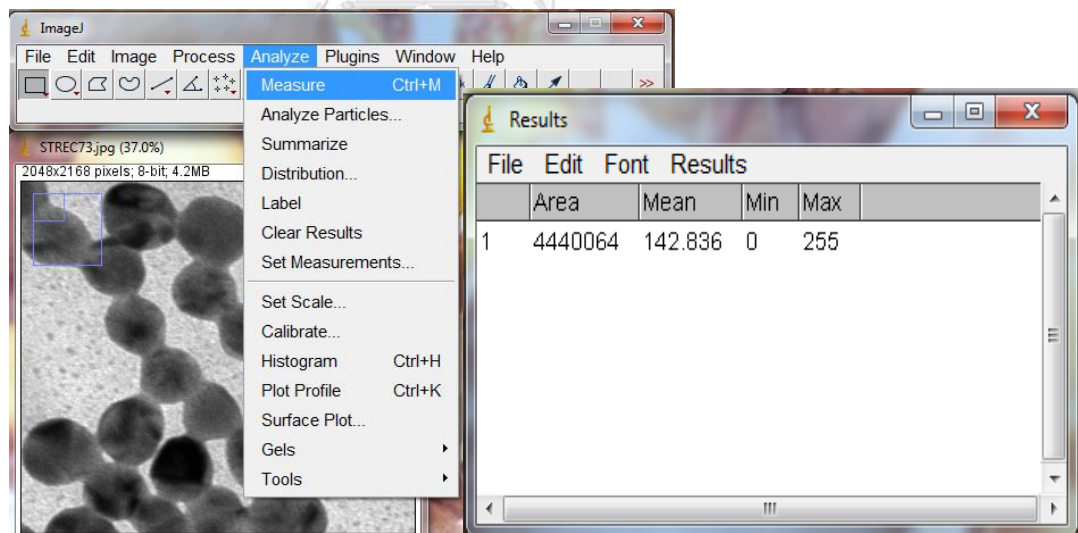
2. Open TEM image of AuNP



3. Set scale for analysis



4. Measure the data



5. Create of size distribution graph

VITA

Miss Chonnicha Subkod was born in Ratchaburi, Thailand on June 4, 1991. She received Bachelor degree of Science from the Department of Biomedical Technology, Faculty of Allied Health Sciences, Christian University of Thailand in 2013. She subsequently enrolled in the degree of Master degree, Program in Biotechnology, Faculty of Science at Chulalongkorn University in 2015.

Academic presentation:

Subkod, C., Puthong, S., Dubas, T, S., Komolpis, K., and Palaga, T. 2017. Enhancing the effect of stapled α -helical mastermind-like 1 (SAHM1) by conjugation with gold nanoparticle against T cell leukemia cell line, Jurkat. Proceedings of 2017 The 29th Annual Meeting of the Thai Society for Biotechnology and International Conference (TSB 2017): Frontiers in Applied Biotechnology, November 23-25, 2017, Swissotel Le Concorde Hotel, Bangkok, Thailand. (Poster presentation)